ESTIMATION OF SHEAR WAVE VIA FEED-FORWARD NEURAL NETWORK AND PETROPHYSICAL BASED THIN BED AVO MODELING OF ZAMZAMA GAS FIELD

DRSM QAU

BY

MARYAM ZAFAR

MPhil Geophysics

2020-2022

Department of Earth Sciences

Quaid-I-Azam University Islamabad

CERTIFICATE

This dissertation is submitted by **Maryam Zafar** D/O **Zafar-ul-Islam** is accepted in its present form by the Department of Earth Sciences as satisfying the requirement for the award of M.Phil degree in **Geophysics.**

RECOMMENDED BY

Dr. Tahir Azeem _____
(Supervisor)

Dr. Aamir Ali _____
(Chairman Department of Earth Sciences)

External Examiner _____

DRSML QAU

ACKNOWLEDGEMENT

In the name of Allah, the Most Merciful and Generous. All thanks be to the Almighty, The One, The everlasting, Who begets no one, is begotten by no one, and has no equivalent. Alhamdulillah. I testify that Holy Prophet Muhammad (PBUH) is the final messenger, whose life serves as a flawless example for all humanity until the Day of Judgment. I am grateful to Allah for the strength and blessing He has given me in finishing this thesis.

Without your assistance, I am nothing. Please keep me prostrated in front of you at all times, and do not allow me to leave in front of anyone else.

First and foremost, I want to convey my heartfelt thanks to my supervisor, **Dr. Tahir Azeem**, for his unwavering support throughout my M.Phil studies and research, as well as his drive, excitement, vast knowledge, and trust in me. I gained a lot of knowledge from his perspective. His advice was invaluable during the research and writing of this thesis.

Dr. M. Raza-ul-Islam (Lecturer, COMSATS University) and **Mr. Yawar Amin** (PhD, Quaid-i-Azam University) have my heartfelt gratitude for their guidance in the preparation of this thesis, as well as their assistance and unconditional support during the two-year journey. And lastly my dear friend **Rana Mujtaba Hussain,** who added page numbers to my thesis.

I really appreciate my entire family's prayers and efforts, particularly my parents and brothers, for their encouragement, support, and sacrifices throughout the study. I'd also like to express my gratitude to the entire staff of my department for providing me with an academic foundation that has allowed me to pursue this course of study.

Maryam Zafar

DRSML-QAU

DEDICATION

I would like to dedicate this research work to my Father (Late), whose affection, love, encouragement, prayers and believe in me made me able to get such success and honor. I hope he is happy up there to see me successful and proud of me. ☺

DRSML QAU

ABSTRACT

Geoscientists continue to be challenged by the complexities of petroleum reservoir systems. Due to a lack of high-quality data, there is a lack of understanding of reservoir dynamics, resulting in inaccurate reservoir potential estimation. .Shear wave velocities have a wide range of applications in petrophysical analysis and in accurate reservoir characterization. Shear wave velocity helps to improve the reservoir and fluid prediction accuracy by decreasing seismic-based uncertainty. However, acquiring S-wave velocity is difficult and costly, resulting in the lack of S-wave velocity data for some gas and oil reservoirs. Therefore, estimation of precise S-wave velocity has become a serious challenge. In this study, three-layer Feed Forward Neural network model (FFNN) in combination with feature importance has been utilized to estimate the shear wave log (DT4S). Prior to neural network application, Feature importance has been to analyze the input data to get optimum results. Out of available 46 logs, 6 logs (DT, LLS, LLD, NPHI, GR, PEFZ) have been chosen for the development of FFNN. The model contains 1 hidden layer containing 16 neurons. 70% data has been used to train the FFNN and remaining 30% data was used for testing. The obtained results (Zamzama-01 well) shows 87% correlation with the measured log. To further check the credibility of this designed network, it was applied on another area where input logs cover the early cretaceous rock. The trained network provides excellent matching (84%) with the measured log. After checking the credibility of designed neural network, DT4S log was also estimated in Zamzam-03, and 05 well where it does not acquired. Estimates DT4S log in combination with other elastic and reservoir parameters were crossplotted in order to distinguish the hydrocarbon bearing zone. The crossplot clearly separate the gas bearing and non-gas bearing zones. Further petrophysical investigation of Zamzama-01, clearly indicate that Pab-sandtone formation comprises of thin sand beds that serve as suitable reservoirs. These beds have good porosity values (11%), low shale volume (12%) and low water saturation (25%). To study these thin beds, three-layer forward AVO model, and wedge modeling have been used. Wedge modeling results indicate that bed having thickness of 26m, 22m, and 19m can be identified if seismic data have dominant frequencies of 25Hz, 30Hz and 35HZ, respectively. Moreover, AVO forward modeling shows Class IV AVO response from the top layer of gas-bearing sand.

DRSML OAU

Table of Contents

DRSML QAU

DRSML QAU

Table of Figures

DRSML QAU

DRSM-QAU

List of Tables

DRSML QAU

CHAPTER 1
INTRODUCTION TO DISSERTATION

1.1 Introduction

Hydrocarbon exploration is one of the most important elements of any country's economy. As the demand for energy grows, the research sector turns its attention to previously unknown locations in search of new energy resources. To examine the ground, geophysical procedures and equipment are utilized, which include taking measurements and computing physical attributes to check for differences both laterally and vertically (Arshad et al., 2013).

Exploration geophysicists began working on the seismic approach in 1915, and it has since shown to be quite beneficial for imaging subsurface geological features and locating structural or stratigraphic traps. Seismic surveys, which portray data as a time series of reflections through the subsurface, are commonly used in hydrocarbon exploration (Coffeen, 1986).

The primary tool for hydrocarbon exploration is 3D seismic interpretation. 3D seismic surveys offer numerous benefits and can be used for a wide range of concerns, from exploration to development. They're also useful for limiting the scope of extensive reservoir characterization (Alsadi, 2017). 3D seismic data can be used to efficiently analyze the subsurface features. When compared to 2D data, the structures may be viewed with high resolution alongside the vertical cross-segment of the earth and its entire volume in 3D data. The amplitude sections reveal the extent and quality of reserves, as well as their formation borders and faults (Raeesi et al., 2012).

Conventional interpretation approaches are typically employed to demarcate large-scale structural traps, however, they are ineffective when dealing with narrow, interbedded reservoirs which are undetectable under the threshold seismic resolution (Farfour et al., 2015). Due to low seismic resolution, amplitude reflections from alternating thin layers frequently experience tuning thickness problems. As a result, amplitude anomalies are taken into account and examined using various approaches such as amplitude versus offset (AVO), amplitude versus angle (AVA), and spectral decomposition (Saeed et al., 2020).

The study of rock characteristics and their interaction with fluids is known as petrophysical analysis. The most significant attribute of fluid for its storage and movement within the rock is

DPSML QAU

porosity and permeability. Because petrophysical logs contain the majority of data, they are utilized to map and identify lithologies (Tiab & Donaldson, 2015). Reservoir characterization is a combination of procedures used to characterize reservoir heterogeneity (Lake & Caroll, 1986). In reservoir characterization, petrophysical analysis is particularly useful for distinguishing hydrocarbon and non-hydrocarbon bearing zones (Yuedong & Hongwei , 2007). In most cases, petrophysical analysis is used to estimate reservoir parameters, including shale volume, permeability, porosity, and water and hydrocarbon saturation, from wireline log data. The ability to distinguish between hydrocarbon and non-hydrocarbon bearing zones can be greatly improved by a thorough examination of these reservoir features (Azeem et al., 2017).

Shear wave velocities have a wide range of applications in accurate reservoir characterization. However, acquiring S-wave velocity is difficult and costly, resulting in the lack of S-wave velocity data for some gas and oil reservoirs. As a result, obtaining a precise S-wave velocity has become a serious challenge. Artificial neural network (ANN) is gaining importance in the fields of geophysics. In geophysics it is preferred due to its low cost and efficient computational time. The ANN is an effective standard tool for nonlinear issues because it is extremely adaptable and capable of developing functional links between data (Singh & Kanli, 2016). The findings achieved by using ANN to build a non-linear relationship between the input and output data is valuable and dependable (Zhu et al., 2012). In theory, the ANN can compute any arbitrary map building between one vector space to another because it has the ultimate power to approximation of data. (Svozil et al., 1997). Neural networking plays an important role in accessing the prior unknown parameters encoded in data (Svozil et al., 1997).

DRSM- QAU

1.2 Study Area

Pakistan's southern and northern regions have a lot of hydrocarbon potential (Alsadi, 2017). The Zamzama gas field is located 200 kilometers north of Karachi in the Sindh region of Pakistan (Qadri, 1995). It has a surface area of 120 square kilometers and ranks fourth in terms of discovered gas resources in Pakistan. It is the eastward progressing thrusted anticline with a huge north-south oriented reverse fault (Jackson et al., 2004).

The Zamzama field is surrounded by the Kirthar range in the west, which consists of a 560 km long and 130-220 km wide belt with a NS direction, containing basins and valleys. Sukkur is in

the NE of the field and district Hyderabad is towards its SE. The river Indus is in the east, and Karachi is located to its south. Lake Manchor is located to the south of the field, close to the Indus River, flowing in the eastward direction. The majority of production comes from late cretaceous Pab Formation fluvial and shallow marine sandstones, as well as estuarine Paleocene Khadro Formation sandstones (Qureshi et al., 2020). For the next 10 to 12 years, the field is estimated to produce roughly 320mmcf/d of gas and 2000 standard barrels of condensate (stb/d), with an economic field life of 15 to 25 years (Jackson et al., 2004).

In the kirthar fold belt, the late Cretaceous Pab sandstone serves as a primary reservoir (Jackson et al., 2004). The Zamzama area is surrounded by other gas field such as, Bhit (southwest of Zamzama), Sawan, Kadanwari, and Maino fields (northeast of Zamzama) are other gas fields located nearby. The entire known recoverable reserves from the core area of the Zamzama field are estimated to be 1.7 Tcf of gas (Jackson et al., 2004).

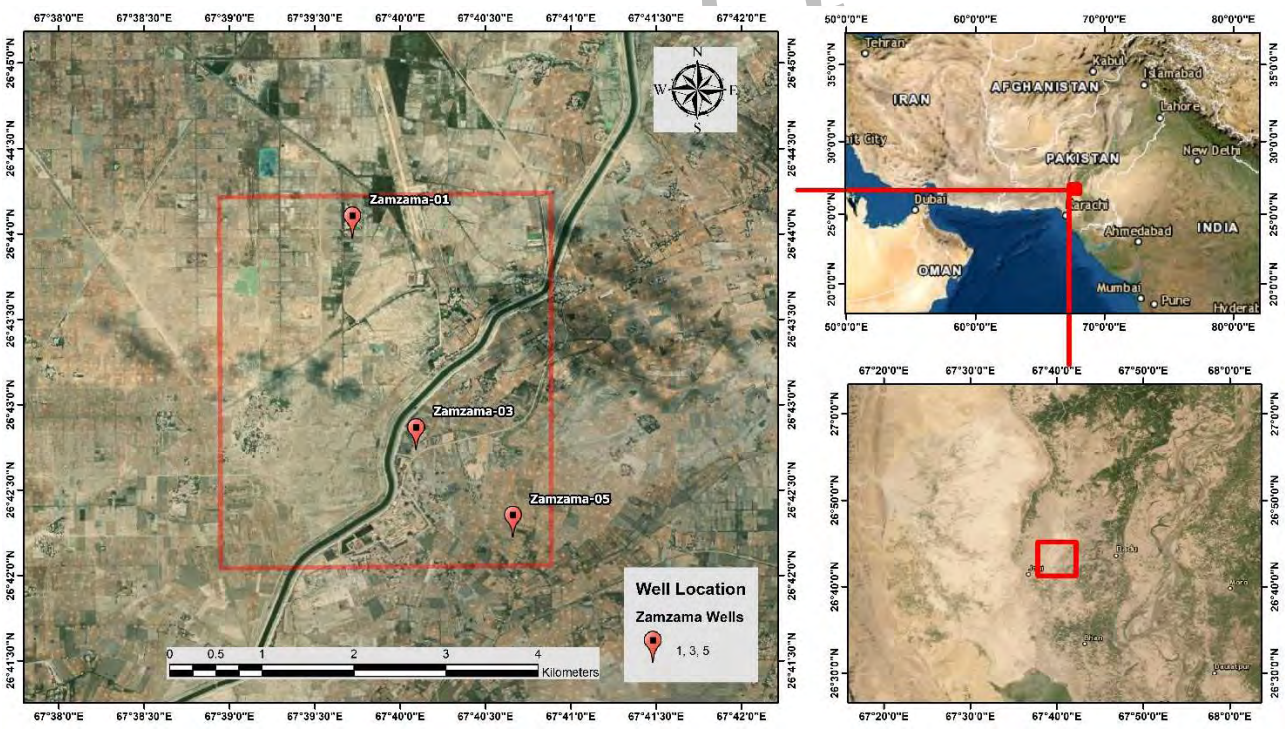

Figure1.1: Map showing the location of wells and orientation of 3D seismic cube in Zamzama gas field

1.3 Main Aims and Objectives

General aims of the current research work are as follows:

- To study the subsurface structures of the study area using 3D seismic interpretation.
- To carry out petrophysical analysis of the reservoir rock in order to identify the potential prospect hydrocarbon zones.
- Estimation of DT4S (Shear Wave) log via feed-forward neural network and subsequently characterize the reservoir using calculated elastic parameters.
- To perform wedge modeling and AVO analysis for identification of thin bedded reservoirs of Zamzama gas field.

1.4 Data Set and Methodology

1.4.1 Seismic Data

The seismic dataset used in the study is given in Table 1.1. 3D seismic cube covering an area of 12x12 km^2 is used in this research work. This cube comprises of 90 inlines starting from 420 to 510 and 180 crosslines ranging from 1320-1440 used in this research.

Table 1.1 Details of inline and crossline of 3D Seismic Data

Lines	Start	End	Total No of Lines
In Line	420	510	90
Cross Line	1320	1440	180

DRSML QAU

1.4.2 Well Log Data

The details of the well log data used for this study is given in Table 1.2. Total of three wells (Zamzama-01, Zamzama-03, and Zamzama-05) were used for research purpose. Out of available logs data, 8 logs i.e. GR, SP, CALI, LLS, LLD, NPHI, DT, and RHOB were used for petrophysical analysis to identify the prospect zone.

Table1.2 Details of wells used in research work

Sr. No	Well Name	Longitude	Latitude	Total Depth
1	Zamzam-01	67.6619	26.7344	3950
2	Zamzama-03	67.6682	26.7138	3698
3	Zamzama-05	67.6706	26.6676	3871

1.4.3 Methodology

The main emphasis of this dissertation is to predict the DT4S log in reservoir zone for accurate reservoir characterization. Prior to the prediction of DT4S log, identification of subsurface geometry is necessary. For this purpose, 3D seismic data and well log data was used. First of all well to seismic tie is carried out to marks the horizons and faults on seismic section. After that, the petrophysical analysis was carried out in the desired reservoir zone to identify the hydrocarbon zone by displaying available logs in lithology, resistivity and porosity tracks. After the identification of reservoir zone, the main part of research was done i.e. prediction of DT4S log. For the prediction of DT4S log, three layered feed forward neural network was utilized in the combination of feature importance. Prior to neural network application, it is necessary to analyze the input data to get optimum results. Feature importance analysis were perfomed and as a result of this, 6 logs (DT, LLS, LLD, NPHI, GR, PEFZ) out of 45 available logs have been chosen for input. After that, designed network was used over different wells to check the credibility of network. After checking the credibility, the designed network was used to estimate the DT4S logs in those wells where, it was missing. Estimated DT4S log was further used for reservoir characterization. In order to distinguish between lithologies in the reservoir zone based on fluid content, calculated elastic parameters have been cross plotted. Finally, three-layer forward AVO model, and wedge model were prepared to analyze the tuning thickness of thin bedded reservoir.

DRSML QAU

1.5 Brief Description of Dissertation

This thesis is split into six chapters, the first of which serves as an introduction. The geologic background is covered in Chapter 2 including a stratigraphic chart with the source, seal, and reservoirs of the research area labeled with various colors. The seismic interpretation of the study

area utilizing seismic reflection methods has been discussed in Chapter 3. Using well-logs, numerous petro-physical parameters estimated for characterizing the reservoir have been discussed in Chapter 4. With the help of neural network, the main purpose of this dissertation has been carried out i.e., prediction of shear wave velocity with the help of petrophysical logs, have been discussed in Chapter 5. Furthermore, it is also includes reservoir characterization done with the help of cross plotting the calculated elastic properties. In Chapter 7, the AVO analysis of thin beds have been discussed.

DRSML QAU

CHAPTER 2
REGIONAL GEOLOGY AND TECTONICS

2.1 Introduction

Geology is the study of evolution of the earth over time. It depicts the earth's history and aids interpretation of the surface and subsurface structures by providing information on deformation, structure types, and rock types. The study of depositional environments proves beneficial in determination of profitable and non-productive zones for hydrocarbon exploration. Therefore, studying the geological history of an area is crucial in the field of oil and gas exploration. Essentially, the geological history of the area is linked to the area's tectonic behavior and deposited sedimentary sequences (Larsen et al., 1992). For precise seismic interpretation, geophysicists must be aware with the regional geology and geology of the location (Sheriff, 1976).

2.2 Structural Style

Pakistan is situated at the intersection of two differing domains. Pakistan's south-eastern region is in the Gondwanian domain, whereas the north-western region is in the Tethyan domain (Kazmi & Jan, 1997). Tethyan domain is found in Pakistan's northernmost regions, including the Karakoram, Kohistan-Ladakh, Kharan, Chagai, and Makran. The Himalayas, Salt Range, Indus Basin, Cholistan, Eastern Ranges of Balochistan, and Thar Desert are all part of the Gondwanian realm, which covers Pakistan's southern half (Kazmi & Jan, 1997).

Open and symmetrical folds dominate the Kirthar fold belt. Thrusts in the Eocene mudstones and thrusts with a deeper detachment in the Lower Cretaceous source rock period that involve the reservoir during deformation defined by horst and Graben structures, as well as a system of trans-current faults, have been interpreted with two detachments north-western region is in the Tethyan domain (Zaigham & Mallick, 2000). A considerable number of anticlinal structures were formed on the eastern side of the Kirther fold belt as a result of plate collision during the Oligocene–Miocene period (Arshad et al., 2013).

. The predicted shortening along the Zamzama structure represents deformation associated to fault propagation folds. This indicates that a decollment exists beneath the structure, resulting in

DRSML QAU

Zamzama being a thin-skinned structure with no basement involvement in the deformation. (Figure 2.1)

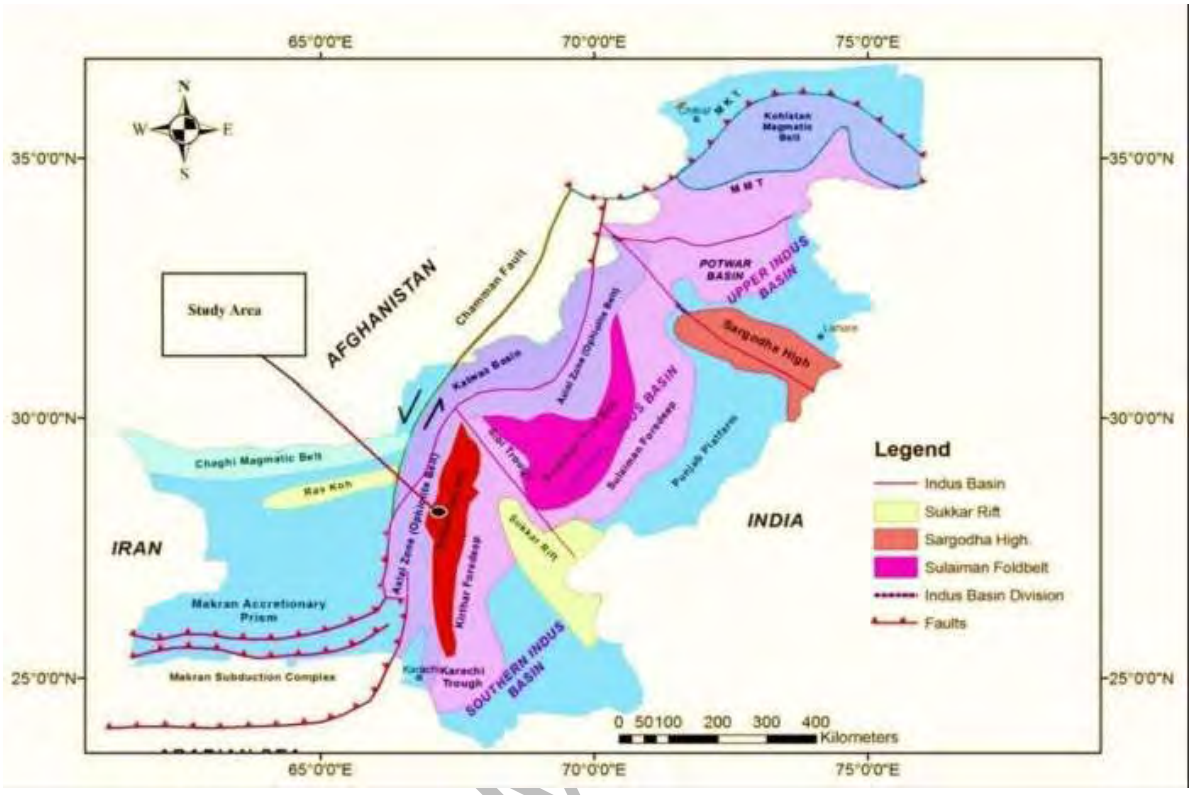

Figure 2.1: structural style of Zamzama Area and it's surrounding (Kazmi & Jan, 1997)

2.3 Geological Setting

The geological environment of a sedimentary basin controls hydrocarbons, migration, and trapping. Gandwanian domain and Tethyan domain are the two territories that make up Pakistan. The Indo-Pak crustal plate supports the southern half of this, which belongs to the Gandawanian domain (Kazmi & Jan, 1997).

This area has rocks, dating from the Triassic to the recent epochs. During the Cretaceous, the Indian plate rifted apart and drifted away, resulting in the formation of the Lower Indus basin. Sedimentary sections from the Tertiary to Mesozoic epochs show respective source, reservoir, and cap rocks (Asim et al., 2014). Sand bodies developed in a variety of shallow marine environments, ranging from shore face to lower shelf marine conditions, make up this formation (Jackson et al., 2004). During the late Cenozoic, the greater influence of clastic debris from the north side

DRSM

compelled the sea to withdraw to the south. The Indus basin was filled with sediments by the end of the Paleocene, and it resembled a large flood plain with braided streams, with the folded belts providing the sole height.

2.4 Stratigraphy and Petroleum Play

The Kirthar Foldbelt Basin have a stratigraphic succession ranging from Permian to Recent, with substantial unconformities at the Permian, Jurassic, and Upper Cretaceous ages (Zafar et al., 2018). The deep Oligocene to quaternary age rocks are found in the Lower Indus Basin, overlain by Mesozoic to Eocene passive edge clastics and carbonate deposits that pierce the tertiary orogenesis of the kirthar fold belt (Figure 2.2) (Qadri, 1995).

The Cretaceous rocks in the surrounding regions of Suleiman and Kirthar provinces of the Lower Indus Basin are largely sedimentary in origin and, with the exception of small disconformities, form a continuous succession from Early to Late Cretaceous. In some portions of this area, the Tertiary layers are transitional, and local disconformities between the Cretaceous and Tertiary have been identified (Zaigham & Mallick, 2000).

A mature source rock, a channel to migrate hydrocarbons, reservoir rock, optimum time for the creation of these elements and the migration processes are all geological processes required to produce and accumulate hydrocarbons (Monreal et al., 2009).

DRSML OAU

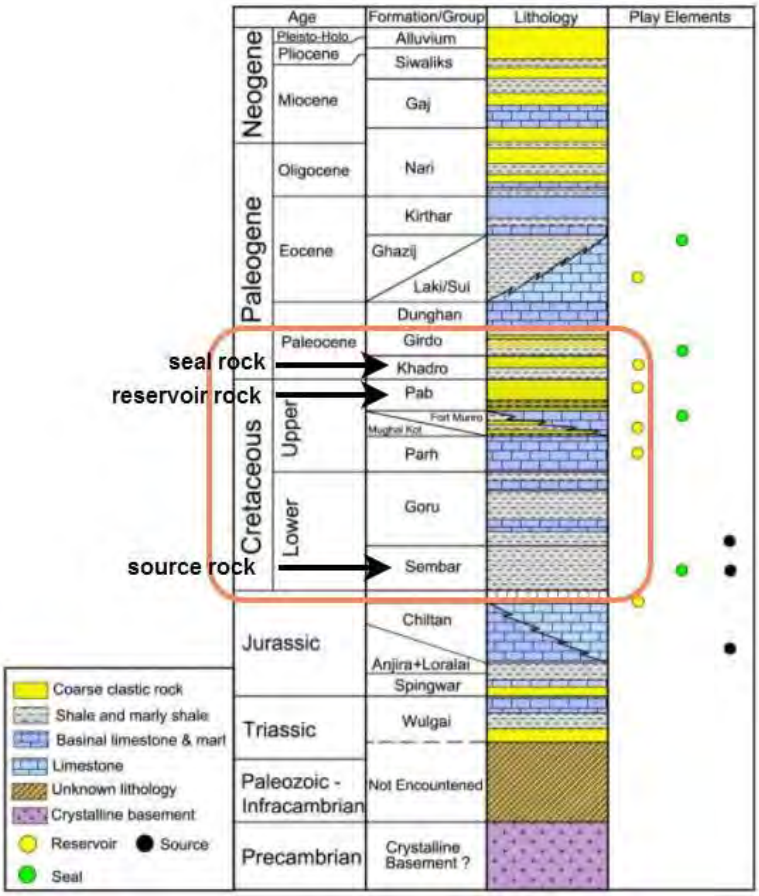

Figure 2.2: Stratigraphic Column of Zamzama area with heighlighted petroleum paly, (Zafar, et al., 2018)

DRSN

2.4.1 Source Rock

Sembar formation of cretaceous age act as source rock in the study area. The Lower Cretaceous Sembar and Goru Formations mostly include gas-prone type-III kerogen. The Sembar Formation shale also contains type-II kerogen, indicating the possibility of oil production (Wandrey et al., 2004).

Goru depicts a pelagic environment, whereas the Sember was found on the shelf edge. The majority of the Sember deposits come from a marine environment (Zafar et al., 2018).

Sembar's TOC ranges from 0.5 to 3.4 percent, with an average of 1.4 percent. Depending on where in the source kitchen to the west, Sembar Formation shales range from thermally immature in structural highs to highly mature (Zafar et al., 2018).

2.4.2 Reservoir Rock

Reservoir rocks that are porous and permeable are deemed economic in terms of hydrocarbon resources. The most essential physical features of reservoir rocks for hydrocarbon accumulation are porosity and permeability (Qadri, 1995). The principal reservoir for the Zamzama field is the Cretaceous Pab Sandstone. It is found in a tidal and shallow marine environment. The Pab sandstone is a braid delta/coastal plain deposited formation that is exceptionally sand-rich. This reservoir has a net thickness of about 220m and a net-to-gross ratio of about 60% (Jackson et al., 2004).

2.4.3 Seal Rock

Shales from the paleocene Khadro and Ranikot formations act as a top seal for the underlying Pab sandstone. These shales have proven to be reliable in Bhit, Zamzama, and Mehar fields, among other places. The underlying Pab Formation is well-sealed by the basal Khadro Formation shales. In some circumstances, Khadro becomes sandier and does not serve as an affective seal, in such situation Gidro provides the seal (Qureshi et al., 2020).

DRSM QAU

CHAPTER 3
3D SEISMIC DATA INTERPRETATION

3.1 Introduction

The earth is extended over three dimensions and the petroleum resources are trapped inside 3D traps. The interpretation of the processed seismic data is followed by hydrocarbon exploration and extraction. Geologic information about the subsurface includes structures, subsurface rock features, stratigraphy, velocity and stresses, and probable reservoir fluid changes in space and time (Onajite , 2013). Interpretation is a method for attempting to identify all the structures or stratigraphical models embedded in the seismic data. We aim to determine the zone of interest by interpreting the seismic section by focusing on the typical geological model of the earth. Not only must a proper interpretation be consistent with all seismic data, but it is also necessary to have a thorough understanding of the field, surface geology, well information, and geological and physical concepts (Sheriff, 1999).

The essential abilities that are widely employed in the oil business for exploration are seismic interpretation and subsurface mapping (Gunderson & Huffman, 2018). Because of its high resolution, the seismic reflection technique is one of the most essential geophysical techniques for petroleum operations. Seismic interpretation is the process of extracting subsurface information from seismic data collected on the earth's surface. It may also be used to estimate the area's overall geological knowledge, as well as to determine locations for future exploratory well or to assess the development of an already discovered field (Coffeen, 1986). Generally, seismic reflection data from acoustic impedance interfaces with lateral continuity has been used to pick and track laterally consistent seismic reflectors for the purposes of mapping geologic structures, reservoir architecture, and stratigraphy (Das et al., 2017).

DRSML QAU

3.2 Structural Analysis

The seismic section is subjected to structural analysis in order to identify prospective structures capable of storing and accumulating hydrocarbons. The interpretation method utilized in the delineation of structures is two–way seismic reflection time rather than depth. The fundamental

concern in this strategy for hydrocarbon buildup is observation of structural entrapment such as anticlines, faults, and folds (Sheriff, 1999).

3.3 Workflow of Seismic Interpretation

Multiple steps were used in the interpretation of the available seismic data. Each phase entails a number of steps that were carried out with the use of software tools. Simplified workflow employed in the dissertation, shown in Figure 3.1, provides a complete picture of how interpretation was carried out using the seismic lines and SEG-Y navigation data using IHS Kingdom. The base map was created. Faults and horizons of interest were demarcated. Horizons were identified using synthetic seismogram derived from well data, and faults were identified using careful examination of seismic sections and knowledge of the research area's geologic history.

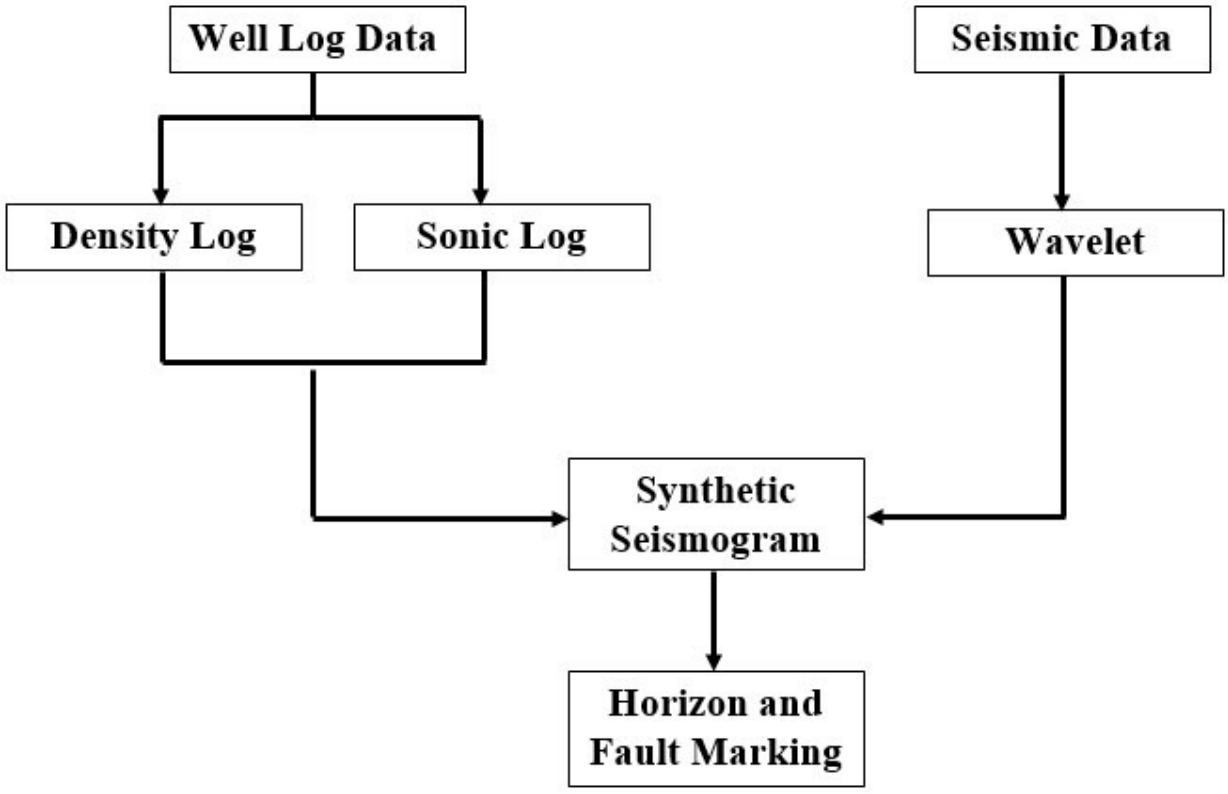

Figure 3.1: Workflow adopted to mark the horizons and faults on seismic section

3.4 Base Map

The base map depicts well locations and orientation of inlines and corss lines. The location of geographic references are often merged into the base maps either by using latitude and longitude values, or in X Y form using Universal Transverse Mercator (UTM) information.

In geophysics, the base map shows the alignment of seismic lines and the locations where seismic data was collected. The base map was constructed using the provided navigation data, which included latitude and longitude values for inlines, crosslines, and Well locations. The base map depicts the locations of all inline, crosslines, and wells in case of a 3D grid. Inlines are oriented across the dip of any regional fault in the area, thus exhibiting information about the structural variation of the vicinity. The crosslines are oriented orthogonal to the inlines. The base map of the study area includes the seismic cube, along with Zamzama-01, Zamzama-03 and Zamzama-05 wells as shown in Figure 3.2.

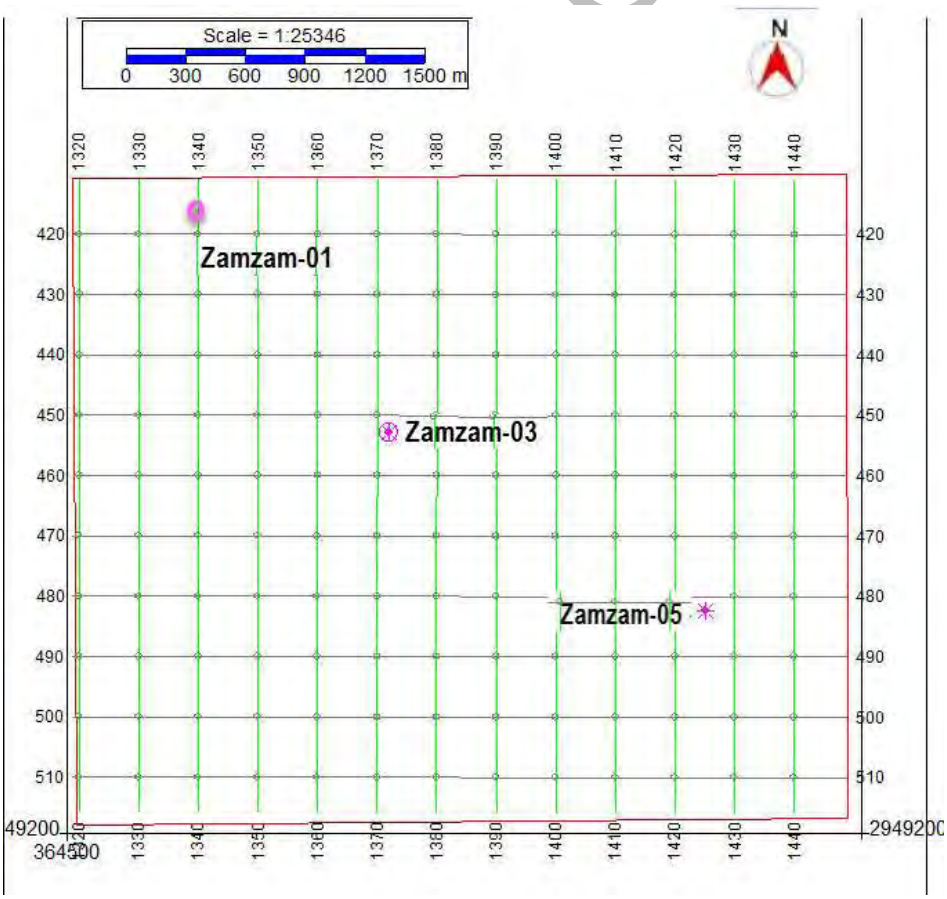

Figure 3.2: Base map depicting inlines, crosslines, and well locations of the study area.

QAU

3.5 Synthetic Seismogram

The creation of synthetic seismograms is used to connect the well to the seismic section. It allows you to spot reflections and figure out which event is related to which interface or series of interfaces. First, the sonic and density logs were used to calculate the reflectivity series (Peterson et al., 2002). The wavelet was then retrieved from the seismic data at the well locations. To obtain the desired synthetic seismogram, the reflection coefficient series was convolved with the extracted wavelet. The Girdo and Pab horizons were demarcated on the seismic section using well tops and generated seismogram (Figure 3.3).

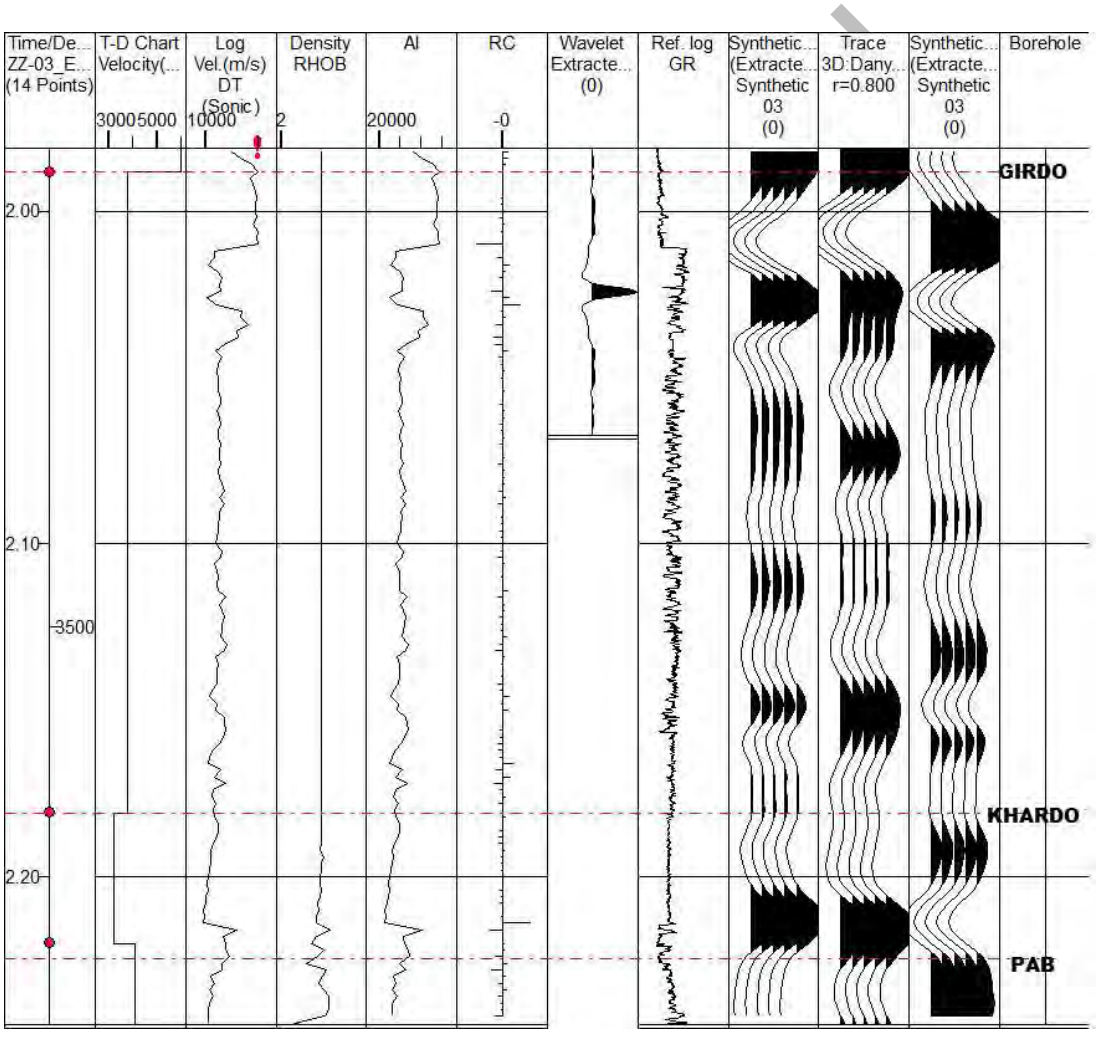

Figure 3.3: Synthetic seismogram for picking horizons on zamzama-03 well.

3.6 Interpretation of Horizons and Faults

Conventional seismic interpretation requires skill and extensive knowledge in geology and geophysics (Wrona et al., 2018). Fault marking on a seismic section is difficult without knowledge of the area's tectonic history (Polo et al., 2017). Horizons are the surfaces that divide distinct rock strata in depositional environments observed on the section based on varying reflection qualities. Horizontal displacement is frequently caused by vertical fractures (faults). Faults are identified during the interpretation process where there is a diminishing amplitude and a shift in the position of the reflectors across the fault. To indicate the exact location of the horizons on the seismic section, the well tops are correlated with the seismic. Two horizons, Girdo and Pab, were interpreted on seismic section based on well tops of Well Zamzama – 03 and two faults, F1 and F2, have been marked, both of which are thrust faults (Figure 3.4).

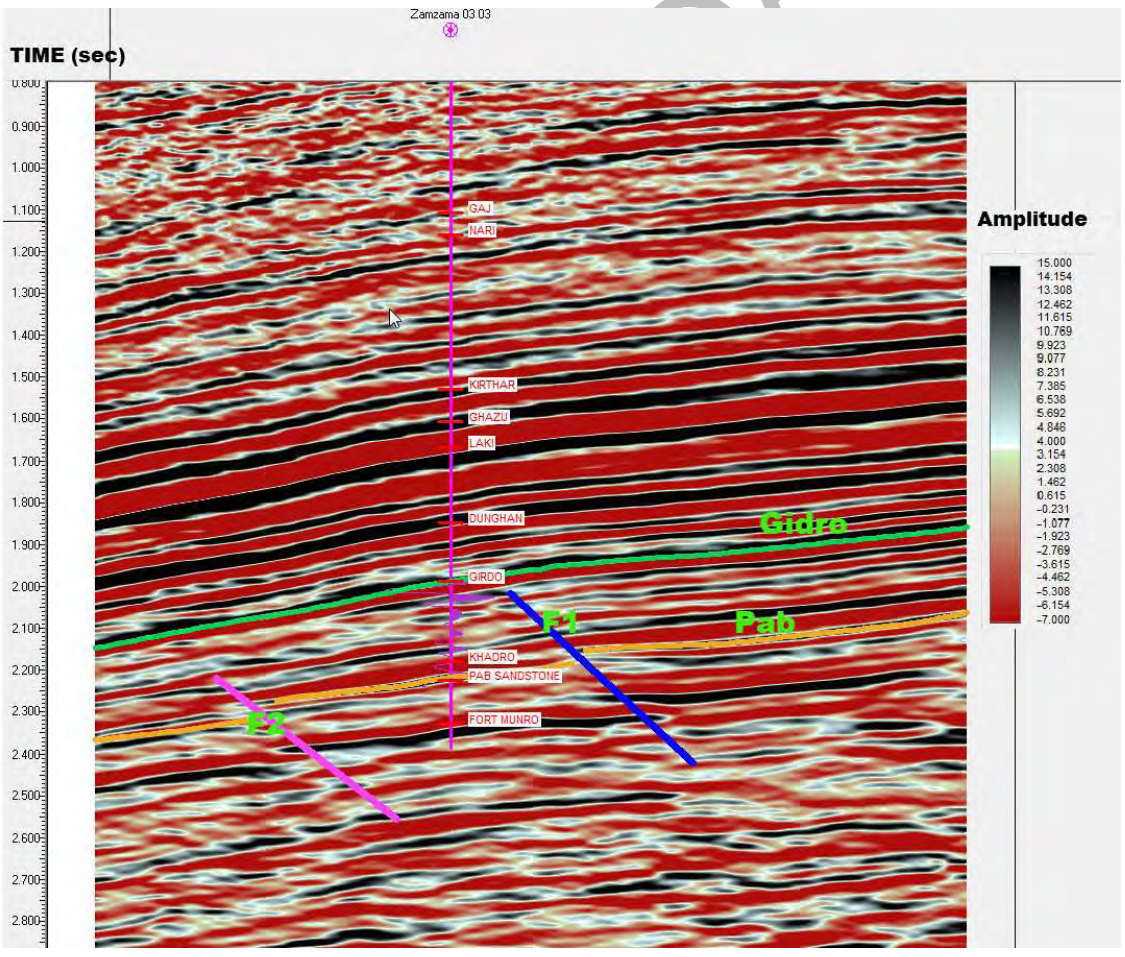

Figure 3.4: Interpreted seismic inline 451 having faults F1 and F2 and two horizons Pab and Gidro

CHAPTER 4
PETROPHYSICAL ANALYSIS

4.1 Introduction

Petrophysics is a field of applied geology that studies reservoir and cap rock properties and their interactions with fluids using fundamental principles of physics, chemistry, and mathematics (Buryakovsky et al., 2012). Reservoir characterization is an important point in the oil and gas business since it aids in determining the potential within the formation of interest as well as identifying the zones within the reservoir that contain retrievable hydrocarbons (Fanchi, 2005).

Petrophysics is a method for estimation and representation of reservoir properties. Petrophysical research aids in the detection and quantification of fluids in reservoirs (Knackstedt et al., 2010) and can be referred to as the interpretation of well logs. Well logging is the art of taking precise measurements of geological and geophysical factors within a borehole. The "Sonde" is a well logging equipment that examines the physical and chemical properties of the rocks as well as their interaction with fluids (Buryakovsky et al., 2012).

Knowledge regarding the characteristics of a reservoir such as shale volume, porosity, saturation of water, and hydrocarbon are essential to precisely delineate the probable hydrocarbon zones. Geologists and geophysicists can better comprehend the hazards and potential in the area by combining petrophysics with rock physics. The use of well measurements to improve reservoir representation has made petrophysics a frequently used method for characterization of reservoirs (Hussain et al., 2017).

DRSML QAU

4.2 Objectives for Log Interpretation

The quantitative examination of well logs can be used for estimation of reservoir parameters including:

- Porosity
- Saturation of water
- Fluid type (oil, gas, water)
- Reservoir type (lithology)
- Productivity (permeability)

The major goals of logging are:

- To acquire data for analyzing petroleum reservoirs.
- To assist in well testing, completion, and rehabilitation.

4.3 Geophysical Well-Logs Classification

4.3.1 Lithology Track

In this track, we have the following logs:

- Gamma ray
- Caliper log
- Spontaneous potential log
- Bit Size

These logs are useful in identification of lithologies as the name of the track suggests.

4.3.2 Resistivity Track

The logs belonging to the second track includes:

- Deep laterolog
- Shallow laterolog
- Micro spherically focused log

These logs are useful in identification of presence of fluid within the formation of interest.

4.3.3 Porosity Track

The following logs comprises the third track:

- Density log
- Neutron log
- Sonic log

The total and effective porosities of a formation can be estimated using any of these logs based on the type of formula being used.

DRSML OAU

4.4 Methodology

The petrophysical examination of Zamzama-1 was completed with the help of the above mentioned logs. The workflow for carrying out petrophysical interpretation has been given in Figure 4.1. The estimated properties of the reservoirs have been listed below:

- Volume of shale (VSH) using the GR log.
- Porosities (PHIT, PHIE) using logs of third track.
- Fluid saturation (Sw, Sh) with the help of logs of resistivity track.

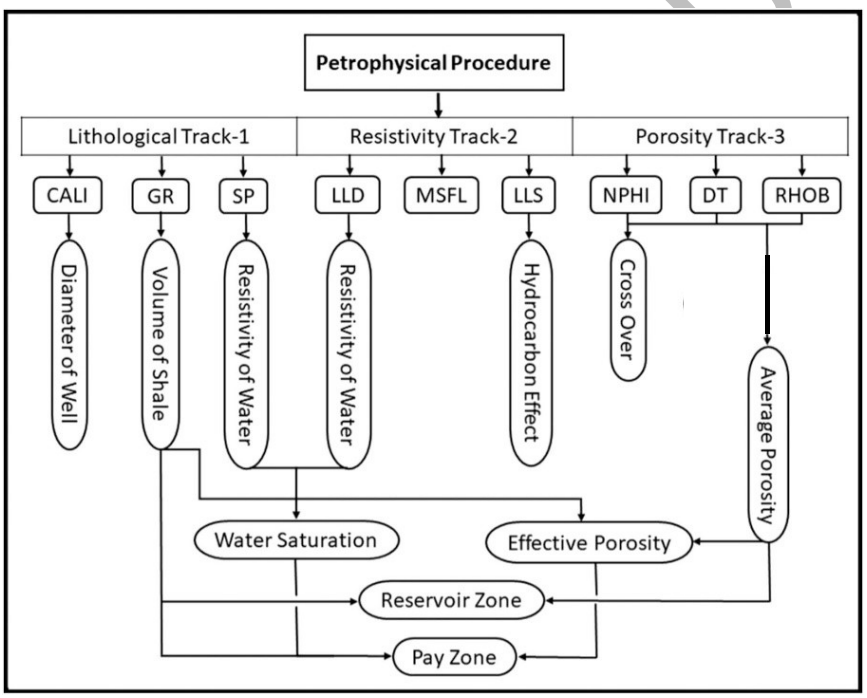

Figure 4.1: Workflow of Petrophysical Analysis, (Mughal & Akhter, 2021)

4.4.1 Shale Volume Calculation

In petrophysical studies, the GR log is used to compute the volume of shale. The radioactivity of the formation is measured using the GR log (Rider, 1990). As a result, it offers the concentration of radioactive material present in the formation, making it extremely valuable for lithology identification. The gamma ray has a low value in carbonate and sandstone, but it has a larger value in shale. The reason for this is because shale has a higher concentration of radioactive material

than sand and carbonates. As a result, the reservoir and non-reservoir rocks are distinguishable (Fanchi, 2005).

The volume of the shale is calculated using the calculations below given by (Miller, 1986)

$$V_{sh} = \frac{GR_{log} - GR_{cln}}{GR_{Shl} - GR_{cln}} \quad (4.1)$$

Here, V_{sh} is volume of shale, GR_{log} is Gamma ray values from log, GR_{cln} is value of gamma ray in clean zone, GR_{shl} is value of gamma ray in shaly zone.

4.4.2 Porosity Calculation

Porosity is the most critical property to estimate when it comes to the petroleum system. Porosity can be calculated using Neutron, Sonic, and Density logs. The acoustic measurement is the sonic log, whereas the nuclear measurements are the Neutron and Density logs (Abdelwahhab & Raef, 2020).

The ratio of pore space to the bulk volume of a rock, expressed in percent, is known as porosity. To some extent, all clastic rocks are permeable. Because compaction is linked to the lowering of pore spaces, pores in sand are particularly relevant in compaction studies. Sonic Log, Density Log, and Neutron Log can be used to determine porosities in the potential zones (Carter & Gregorich, 2007). There are various sorts of porosities, which are listed as follows:

4.4.2.1 Average Porosity

It is the average of all porosity records in the available well log data suite (including Neutron, Sonic, and Density porosity).Its mathematical equation is given below:

$$\emptyset_{avg} = \frac{\emptyset_d + \emptyset_n}{2} \quad (4.2)$$

Here, $\emptyset_{avg}$ is total porosity, $\emptyset_d$ is porosity from density log, and $\emptyset_n$ is porosity from Neutron log.

4.4.2.2 Effective Porosity

Effective porosity is defined as the ratio of total volume of rock body to total volume of interconnected pores spaces that are present in the rock unit. It therefore removes the porosity contributed by shales in the rock. Effective porosity is used to calculate hydrocarbon and water

DRSML QAU

saturation. The formula provided in equation 4.3 is used to calculate effective porosity (Asquith & Krygowski, 2006).

$$\emptyset_{ef} = \emptyset_{avg} * (1 - V_{sh}) \quad (4.3)$$

Here, $\emptyset_{ef}$ is effective porosity, $\emptyset_{avg}$ is average porosity, and V_{sh} is volume of shale.

4.4.3 Saturation of Water

The water resistivity is calculated after the calculation of shale volume and porosities. For the calculation of saturation of water, it is necessary to calculate the resistivity of water first (Patchett & Rausch, 1967).

Different methods can be applied for calculating the resistivity of water. First step for the calculation of water saturation is the calculation of water resistivity. Following are the steps for the calculation of saturation of water:

STEP 1: firstly, we have to note the values of resistivity of mud filtrate (R_{mfl}), Surface temperature (ST) and maximum recorded temperature (BHT) from well's header.

Now, static spontaneous potential can be calculated by the equation given by (Miller, 1986) using spontaneous potential log readings.

$$SSP = SP_{cln} - SP_{shl} \quad (4.4)$$

STEP 2: formation temperature is also required to calculate water saturation. Formation temperature can be calculated using the following equation (Miller, 1986):

$$FT = \frac{BHT - S}{TD} * FD \quad (4.5)$$

FD= Formation Depth

TD= Total Depth

STEP 3: resistivity of mud filtrate can be calculated by the following equation (Miller, 1986):

DRSML QAU

$$R_{mf2} = \frac{(ST+6.77)*R_{mf1}}{(FT+6.77)} \quad (4.6)$$

ST= Surface Temperature

FT= Formation Temperature

STEP 4: mud equivalent resistivity can be calculated by the given formula as (Miller, 1986):

$$R_{mfeq} = 0.85 * R_{mf2} \quad (4.7)$$

STEP 5: equivalent water resistivity can be calculated with the help of spontaneous potential log.

The value against the R_{mfeq} at SSP and BHT gives us the equivalent water resistivity.

STEP 6: from the plot of R_{weq} and formation temperature, we can get the value of resistivity of water (R_w). After getting all the values, saturation of water can be calculated with the help of Indonesian equation for water saturation. Indonesian equation is applicable for the area having sand shale lithology. The calculation is given by (Sam-Marcus et al., 2018) as:

$$S_w = [\{(\frac{{V_{sh}}^{2-V_{sh}}}{R_{sh}})^{1/2} + (\frac{\varphi_e^m}{R_w})^{1/2}\}^2 R_t]^{-1/2} \quad (4.8)$$

R_t= True Resistivity

V_{sh}= Volume of Shale

R_{sh}= Resistivity of Shale

R_w= Resistivity of Water

$Ø_e$= Effective Porosity

m = Cementation factor (varies around 2).

DRSML QAU

4.4.4 Hydrocarbon Saturation

Hydrocarbon saturation represents the presence of hydrocarbon in the pore spaces of rocks. Saturation can be calculated by subtracting the saturation of water from 1 (Kamel & Mabrouk, 2002) as:

$$S_{hc} = 1 - S_w \quad (4.9)$$

S_{hc}= Saturation of Hydrocarbon

S_w= Saturation of Water

4.5 Log Interpretation Criteria

Combination of well logs curves is used for log data analysis. The first log to observe is Calipper log. If the readings of caliper log are not disturbed, then others are obsrved. Second log is Gamma ray log, which can help distinguish between reservoir and non-reservoir zone. The reservoir and non-reservoir zone are therefore highlighted on the basis of gamma ray. This narrows down the area for further interpretation. The region where the shale values are low within a reservoir is selected for analysis. The integrative findings from other logs produce a comprehensive report to confirm the types and amounts of hydrocarbon. Then, we go for SP log, is SP show deflection, presence of fluid will be confirmed.

Hydrocarbon detection is done using resistivity logs which can effectively detect the presence of fluid within the zone of interest. The fluid is detected within the formation based on the difference in the values of LLS and LLD log which otherwise follow the same pattern. Typically, presence of oil and dense gas causes an increase in the LLD values, which are used for observation of resistivity in virgin zone, compare to the LLS values, which are used to investigate the shallow, transition or flush zone. Higher density is associated with extremely low resistance. It could be caused by the presence of heavy minerals such as gluconate, siderite, chlorite, and chamosite etc.

The crossover created between the decreasing values of neutron and density logs is another good indicator of the existence of hydrocarbon (Miller, 1986). Evaluation of the above mentioned indicators have been used to demarcate the zone of interest in the reservoir as depicted in Figures 4.2-4.4.

DRSML QAU

4.5.1 Interpretation of Zamzama-01

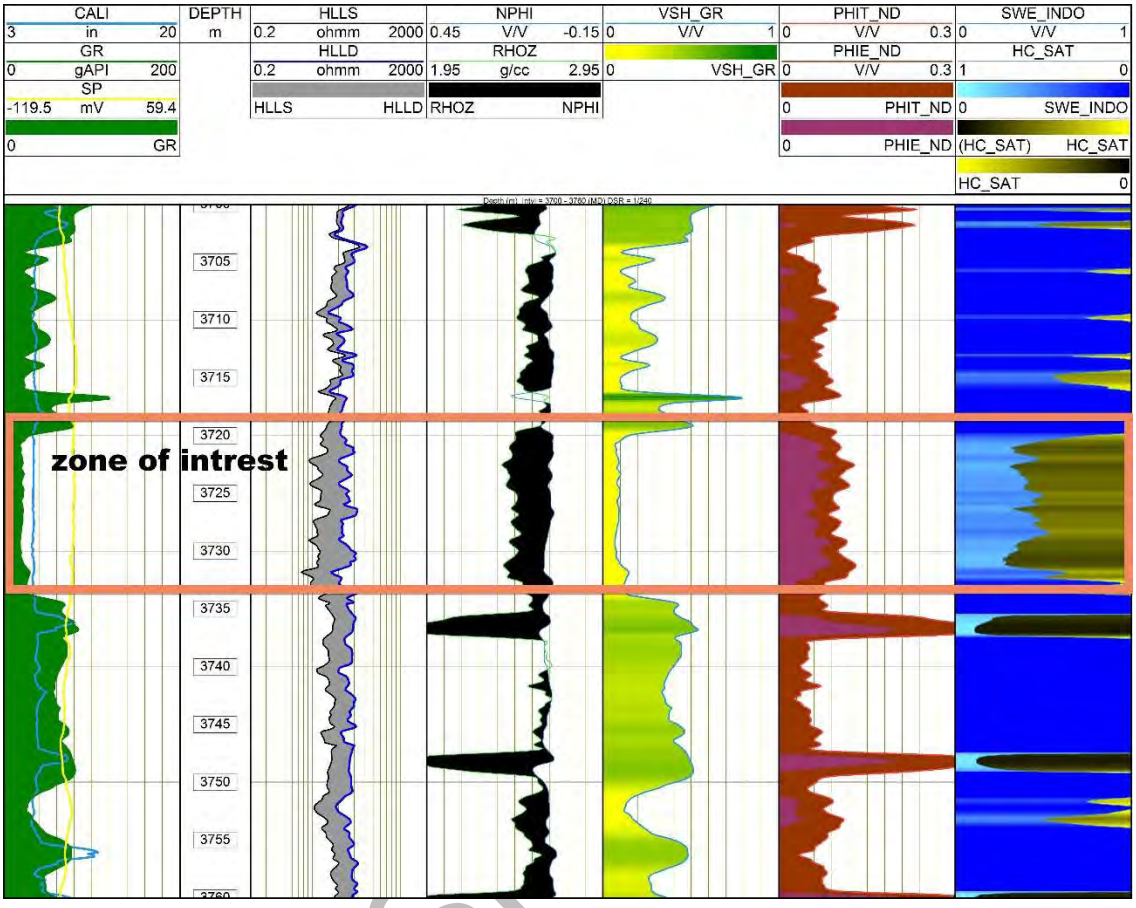

Figure 4.2: Petrophysical analysis of Zamzama well-01

Petrophysical analysis indicates the Zamzama-01 contains a 13m gas bearing zone as shown in figure 4.2. The depth of this zone is ranging from 3720-3733m. Overall, this zone contain low volume of shale (10%) and comparatively high porosity which is 11% in this zone. Further, saturation of water is 25% which is on lower side. However, above or below of this zone the shale volume and water saturation is on higher side. Whereas, effective porosity is on lower side. So, these zones are not favorable for hydrocarbon accumulation.

4.5.2 Interpretation of Zamzama-03

According to petrophysical research, the Zamzama-03 has an 11-meter gas bearing zone, as shown in figure 4.3. The depth of this zone varies between 3790 and 3801 metres. In general, this zone has a low volume of shale (15%) and a relatively high porosity (9%). Furthermore, the water saturation is 30%, which is on the low side. Below this zone, we have low volume of shale but we

don’t have good effective porosity. So, that is why these zoned are not good for hydrocarbon accumulation.

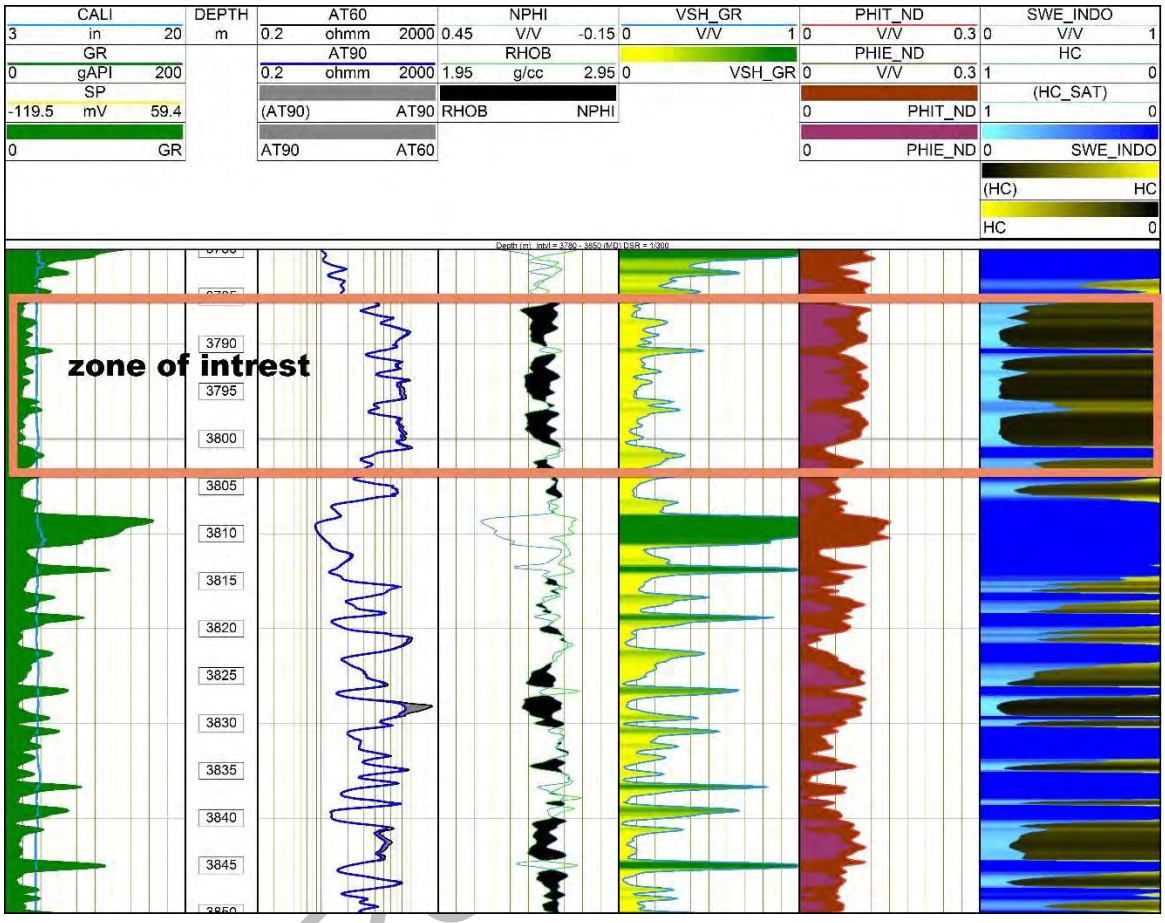

Figure 4.3: Petrophysical analysis of Zamzama well-03

4.5.3 Interpretation of Zamzama-05

The Zamzama-05, as illustrated in figure 4.4, has a 10-meter gas bearing zone, according to petrophysical analysis. This zone's depth is between 3755 and 3765 metres. In general, this zone contains a low volume of shale (12%) and has a high porosity (9%). Furthermore, the water saturation level is 32 %. Low volume of shale has been observed throughout Zamzama well-05, with high effective porosity and NPHI and RHOB crossover, but these zones are in patches and have no economic significance.

Comparison of all the zone of interest in all the three wells has been given in Table 4.1.

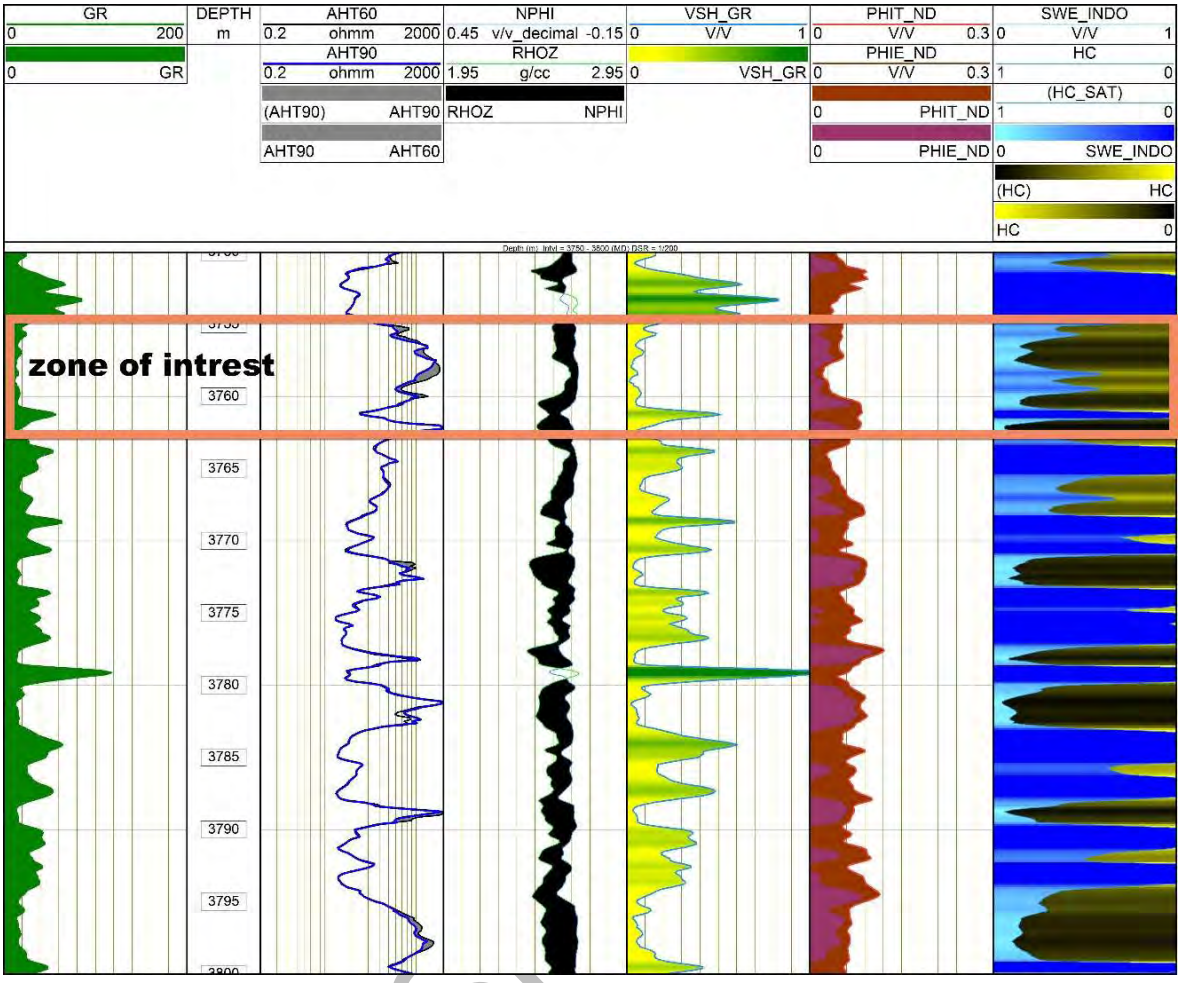

Figure 4.4: Petrophysical analysis of Zamzama well-05

Table 4.1 Results of Petrophysical Analysis

Well names	Zamzama-01	Zamzama-03	Zamzama-05
Gross thickness	3720-3733 (13m)	3790-3801 (11m)	3755-3765 (10m)
Volume of Shale	10%	15%	12%
Effective Porosity	11%	9%	9%
Water Saturation	25%	30%	32%
Hydrocarbon Saturation	75%	70%	68%

DRS

CHAPTER 5
PREDICTION OF SHEAR WAVE VIA FEED FORWARD NEURAL NETWORK AND RESERVOIR CHARACTERIZATION

5.1 Introduction

The intrinsic complexities of petroleum reservoir systems continues to provide a challenge to geoscientists (Al-Anazi & Gates, 2010). Due to a lack of substantial-quality data, there is an insufficient understanding of reservoir behavior resulting in poor estimation of reservoir potential (Akhundi et al., 2014). Shear wave velocities have a wide range of applications in petrophysical analysis, geomechanical research, seismic modeling, amplitude variation with offset (AVO) analysis, and engineering applications (Castagna et al., 1985). The use of a combination of P-wave velocity and S-wave velocity can increase reservoir and fluid prediction accuracy while reducing the seismic based uncertainty (Zhang et al., 2021). However, obtaining S-wave velocity is difficult, time-consuming, and expensive, resulting in the unavailability of S-wave velocity data for some gas or oil reserves. As a result, acquiring an accurate S-wave velocity has become a major challenge (Akhundi et al., 2014).Various empirical relationships for calculating shear wave velocity have been provided by many scientists but the outcomes of these relationships are often inaccurate when used in different regions primarily due to the anisotropic nature of the earth. Furthermore, many factors influence shear wave velocity, but not all of them are considered while developing the empirical relationships. Empirical relationships are generally specific to a certain place or reservoir rock (with specific lithology and fluid), and implementing them to other areas do not yield satisfactory result. The rock and fluid parameters vary from rock to rock and most shear wave velocity measurements have been performed on sandstones, with only a few studies looking for carbonates (Akhundi et al., 2014). Shear wave velocities or moduli from available compressional velocities or moduli can be calculated either empirically or mathematically (Zhang et al., 2021)

Many experts are currently working on relevant studies on S-wave velocity prediction using various methodologies. Castagna, et al., (1985), for example, estimated empirical S-wave velocity formulas for sandstone reservoirs. (Xu & Payne, 2009) Suggested S-wave prediction rock physics model for sandstone reservoirs as well as, for carbonate reservoirs. Russell et al., (2003), Wang et

DRSML-OAU

al., (2020), and Ghorbani et al., (2012) used many neural networks and other machine learning approaches based on well logs to estimate the S-wave velocity.

The deep learning (DL) approach is a new direction in traditional Machine Learning Techniques (MLTs), which uses a series of hidden layers to achieve high-level features from the input information. While traditional MLTs were a point-to-point prediction model based on well logs and did not include the time series characteristics of well logs, the DL approach is a new direction which uses a series of hidden layers to achieve high-level features from input data (Fang et al., 2020). During the interpretation process, a single sampling point cannot adequately reflect the lithology and porosity of the reservoirs. As a result, traditional machine learning algorithms are limited in their ability to forecast S-wave velocity (Wang et al., 2021).

The Artificial Neural Network (ANN) is being applied in a variety of geophysical domains. It is widely preferred since it saves the user time and money. The ANN is an effective standard tool for nonlinear issues because it is extremely adaptable and capable of developing functional links between data (Singh & Kanli, 2016). The findings achieved by using ANN to build a non-linear relationship between the input data and the output parameter are highly reliable (Zhu et al., 2012). In theory, a neural network has the power of a universal approximator, which means it can perform any arbitrary mapping from one vector space to another (Svozil et al., 1997). The ability to access some priori, unknown information encoded in data is the main advantage of neural networks (Svozil et al., 1997).

The neural network is cognizant of the expected outcome and the weight coefficients are therefore modified in supervised training (for example, multi-layer feed-forward (MLF) neural network). As a result, the computed and intended outputs are as close as practically possible to each other (Svozil et al., 1997). ANNs are capable of adapting without the user's help. A neural network is non-linear in and of itself. Nonlinearity is a crucial quality, especially when the relationship between input and output is intrinsically non-linear (Ilonen et al., 2003). Each example in supervised training has a unique input signal and the accompanying target response. MLF neural networks are particularly robust, meaning that their performance diminishes gradually with increase in noise (Sanger, 1989).

DRSML OAU

Prior to neural network application, it is necessary to analyze the input data to get optimum results. Certain tests are applied to reduce the number of input parameters. Gamma test (GT), principal component analysis (PCA), forward selection (FS), and Feature importance (FI) are the techniques used for this purpose (Noori et al., 2011).

Feature importance has become a significant study topic as a fundamental step in data preprocessing (Zhou et al., 2021). Filtering, encapsulation, and embedded feature selection methods are few among the many available (Ball & Brunner, 2010, Tang & Peng, 2017). A common embedded feature selection approach is the decision tree which is frequently used in machine learning and data mining (Zhou, et al., 2021, Sun & Hu, 2017). It has the ability to remove irrelevant attributes while keeping certain key ones in the data. As a result, we may enhance classification quality and speed up the model generation process by using it (Zhou, t al., 2021). In each node, the Decision Tree algorithm always discovers the most significant attributes (Iqbal et al., 2012).

5.2 Data Set

Among the many wells located in the study area, only Zamzama-01 has been used for training of neural network because it has the complete suite of required logs including gamma ray, neutron porosity, density, resistivity, sonic and particularly shear wave log as highlighted in Table 5.1. There are a total of 35 logs run in this well.

Table 5.1 Input Data for Neural Network

Logs Name	Starting Depth (m)	Ending Depth (m)
CALI	**3550.044**	**3929.919**
CALS	1279.169	3317.044
CGR	3323.669	3905.669
DT	**3323.794**	**3570.044**
DT4P	3484.044	3905.669
DT4S	3484.044	3901.294
DTCO	3484.044	3905.669
DTL	1279.169	3317.044
DTLF	1279.169	3317.044
DTLN	1279.169	3317.044
DTRP	3484.044	3905.669
DTRS	3484.044	3898.169
DTSM	3484.044	3905.669
DTTS	116.6642	3901.294

DRSML QAU

GR	**8.9189**	**3929.669**
HCAL	3323.544	3569.919
HDRA	3550.044	3939.919
HLLD	**3323.544**	**3924.794**
HLLS	**3323.544**	**3924.919**
LLD	1279.169	3317.044
LLS	1279.169	3317.044
MSFL	1279.044	3317.044
NPHI	**3323.669**	**3939.794**
DTTP	3484.044	3901.294

RHOZ	3323.544	3939.919
RHOX	3323.544	3919.794
PEFZ	3550.044	3934.919
SGR	3323.669	3905.669
SP	1279.169	3929.669
THOR	3323.669	3905.669
TPRA	3323.669	3905.669
TURA	3323.669	3905.669
UPRA	3323.669	3905.669
URAN	3323.669	3905.669

A large amount of data has been used in training to develop a realistic neural network i.e. around 70% of the whole data, while remaining 30% has been used for testing of the developed neural network. The diagram for logs based neural network is shown in Figure 5.1

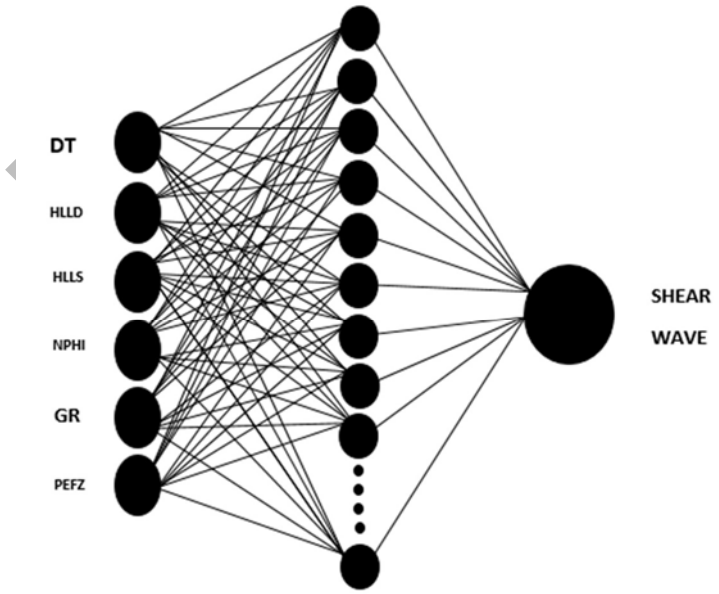

Figure 5.1: Three layer Feed-forward Neural Network Model

5.3 Feature Importance

Feature importance techniques assign a score to input features based on how helpful they are at predicting a target variable (Rajbahadur et al., 2021). Feature significance scores are important because they provide insight into the data, information into the model, and the foundation for feature selection and dimensionality reduction, which can improve the efficiency and efficacy of a predictive model for the problem (Hossain et al., 2020).

Decision tree, statistical correlation scores, permutation importance scores, and coefficients generated as part of linear models are some of the most common types and sources of feature importance scores (Brownlee, 2020).

Extra Decision Tree is a supervised machine learning technique that creates the vertical and horizontal link between each input feature and output feature. It then calculates the relevance scores by deleting each input feature one at a time.

The mathematical representation of feature importance is given by (Ronaghan, 2018) as follow:

$$n_{ij} = w_j c_j - w_{left(j)} c_{left(j)} - w_{right(j)} c_{right(j)} \quad (5.1)$$

n_{ij}= node importance

w_j= weights of nodes

c_j= impurity

Impurity increases with increase in information since information gain is a measure of impurity. "Information Gain" splits the data using entropy. It is calculated by equation given by (Ronaghan, 2018) as:

$$Gain(T, X) = Entropy(T) - Entropy(T, X) \quad (5.2)$$

T= target value i.e. shear wave velocity log.

X= feature to be split on.

DRSML QAU

Entropy (T,X)= the entropy calculated after the data split on feature X.

In a decision tree algorithm, importance of every feature can be calculated as given by (Ronaghan, 2018):

$$fi_i = \frac{\sum_{j:node\ j\ splits\ on\ feature\ i} ni_j}{\sum_{k \in all\ nodes} ni_k} \quad (5.3)$$

fi_i= importance of feature i.

ni_j= the importance of node j.

In this work, the sonic shear wave velocity (DT4S) is predicted through machine learning algorithms by providing the various well logs as input features and DT4S as target feature. The well logs along with input features and target feature are subjected to K fold cross validation. K fold cross validation is the resampling procedure that splits the well logs into the subsamples of equal sized training and testing datasets and subsequently train the model on sample of equal sized training data followed by validation of the model on sample of equal sized testing data (Hossain et al., 2020). The K fold is nominated as 4 which means that K fold cross validation generates the sample of training and testing datasets four times. It then trains the model on training data four times followed by four times validation of the model through determining the correlation between the testing data and predicted data. Extra Decision Tree is a supervised machine learning algorithm that develops the vertical and horizontal relationship between each input feature and output feature and calculate the importance scores by removing the input feature one by one.

The samples of training data and testing data which provides the high correlation is chosen for determining the importance of well logs and the feature importance of each feature is estimated by different estimators and then feature importance is normalized into the single value with the help of standard deviation.

The highest correlation is 83.5 %, achieved from third sample of training and testing datasets and feature importance of each estimated feature is shown in Figures 5.2 and Table 5.2

DRSML QAU

Table 5.2 Correlation values of each input w.r.t output

Sr No.	Log Name	Importance
1	GR	0.152588
2	NPHI	0.237792
3	PEFZ	0.176320
4	HLLD	0.196803
5	HLLS	0.121200
6	DT	0.115296

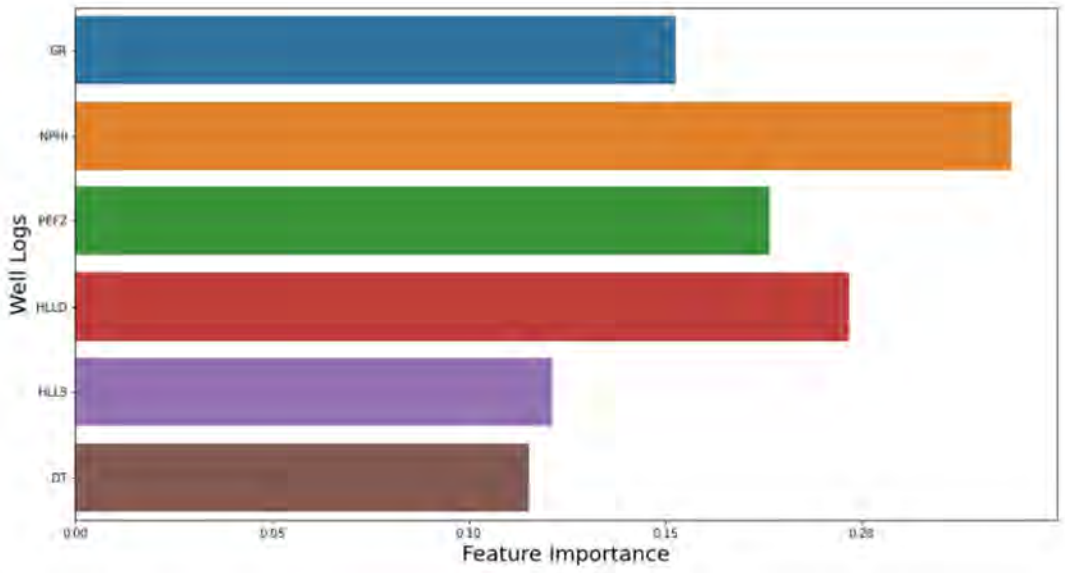

Figure 5.2: Graphical representation of correlation values of each input w.r.t output

5.4 Feed-Forward Neural Network

From the input to the output layers, FFNNs have a one-way link. Prediction, pattern recognition, and nonlinear function fitting are the most prevalent applications. Feed Forward back-propagation, Feed Forward input-delay back-propagation, cascade-forward back-propagation, perceptual, and linear networks are all supported FFNNs (Mahmood & Ahmad, 2017).

A multi-layer feed-forward neural network has the advantage of learning under supervision, therefore enabling it to generate a specified output. As a consequence, the weight coefficients are

adjusted to reduce the difference between the calculated and intended outputs (Hampson, et al., 2001).

The main aim of feedforward neural network training is to determine ideal connection weights (w*) so that the estimated outputs for each sample matches the value of the outputs that are desirable. Typically, this is a non-linear optimization problem.

Where w* is given by (Konate et al., 2014) as follows:

$$w* = \arg minE(w) \quad (5.4)$$

w =weight matrix

$E(w)$=objective function on w

$E(w)$ can be calculated at any point of w using the following equation given by (Konate et al., 2014).

$$E(w) = \sum_p E_p\,(w) \quad (5.5)$$

Where

p=number of examples in the training set.

$E_P(w)$= output error for each example p.

$E_P(w)$ is expressed by following equation (Konate et al., 2014).

$$E_P(w) = \frac{1}{2}\sum_j (d_{pj} - y_{pj}(w))^2 \quad (5.6)$$

For the p_{th} example, the estimated and desired network outputs of the jth output neuron are $y_{pj}(w)$ and d_{pj}, respectively.

To minimize the objective function following equation is used (Konate et al., 2014).

$$\mathrm{E(w)} = \frac{1}{2}\sum_p \sum_j (d_{pj} - y_{pj}(w))^2 \quad (5.7)$$

DRSML QAU

The network calculated output value is compared to the desired output value for each learning (training) operation. If the estimated and desired output networks differ, the synaptic weights that contribute to a major error will be modified more than the weight that contributed to a minor error (Konate et al., 2014).

A three-layer Feed Forward neural network model is utilized with 6 neurons in the input layer, 16 neurons in the hidden layer, and 1 neuron in the output layer. Only one hidden layer is utilized in this network. The hidden layers are utilized to boost nonlinearity and modify the data representation for better function generalization.

The data sample is given into the model in which DT4S represents the dependent output variable. While, DT, HLLD, HLLS, GR, NPHI, and PEFZ represent a single array comprised of six independent variables. The data sample is divided into a training dataset and a testing dataset in order to apply the neural network. The whole dataset was divided into two parts: a training dataset (70%) and a testing dataset (30%) in case of Zamzama-01 (Figure5.3) and Sawan (Figure 5.4) wells and the results were compared.

DRSML QAU

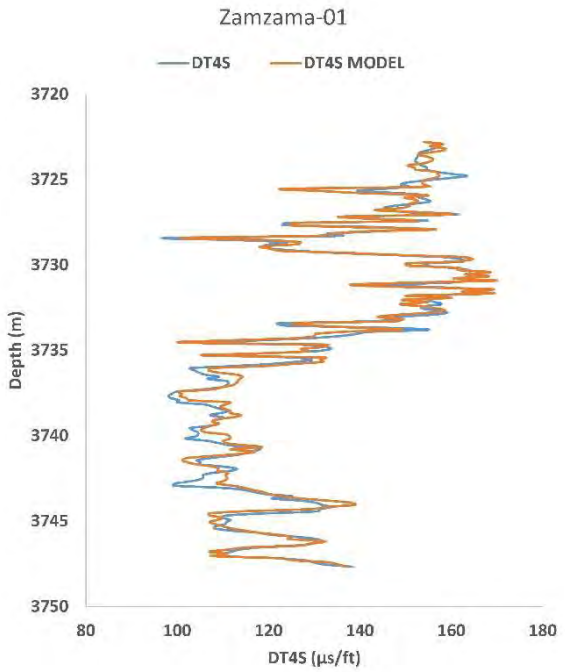

Figure 5.3: Correlation between DT4S and DT4S_MODEL estimated by feed-forward neural network of Zamzama-01 Well

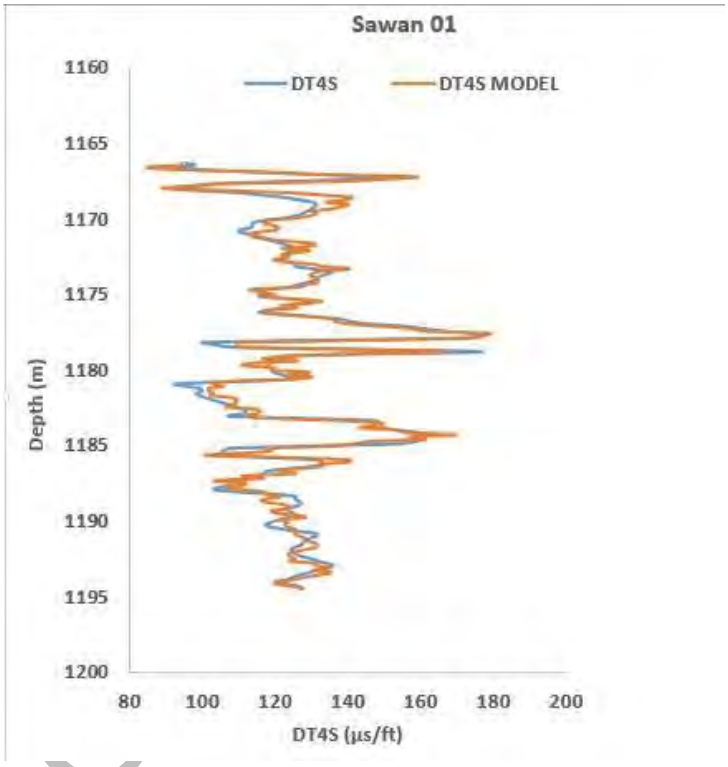

Figure 5.4: Correlation between DT4S and DT4S_MODEL estimated by feed-forward neural network of Sawan-01 Well

Neurons in the input layer do not do any computations because they are simply nodes in the input layer. Biases and weights are related to neurons in the preceding layer by neurons in the output layers and hidden layers. Each neuron in the previous layer sums the weighted and biased input from the previous layer's neurons, then filters the sum with a transmission function (Suzuki, 2011).

The network, which connects each of the neurons until some performance criterion is met, constantly updates the weights and biases to accurately map the inputs into the outputs (Singh & Kanli, 2016).

The weights are optimum when the prediction error is minimized, that is when the predicted value for each training point is as near to the actual value as possible. There are multiple local minima in this non-linear optimization problem.

To determine the global minimum, MLFN employs a combination of conjugate-gradient analysis and simulated annealing. Each of the total iterations consists of a conjugate gradient analysis pass followed by a simulated annealing effort to find an ideal starting point. While there is some trial

DRSML

and error involved in determining the best configuration of middle nodes, the MLFN technique has been demonstrated to be capable of great performance. As a result, MLFN is favored (Latimer, et al., 2000). Figure 5.3 shows that the match between actual DT4S and the ANN measured DT4S is nearly perfect at all depths. It gives us 87% correlation as shown in Figure 5.5.

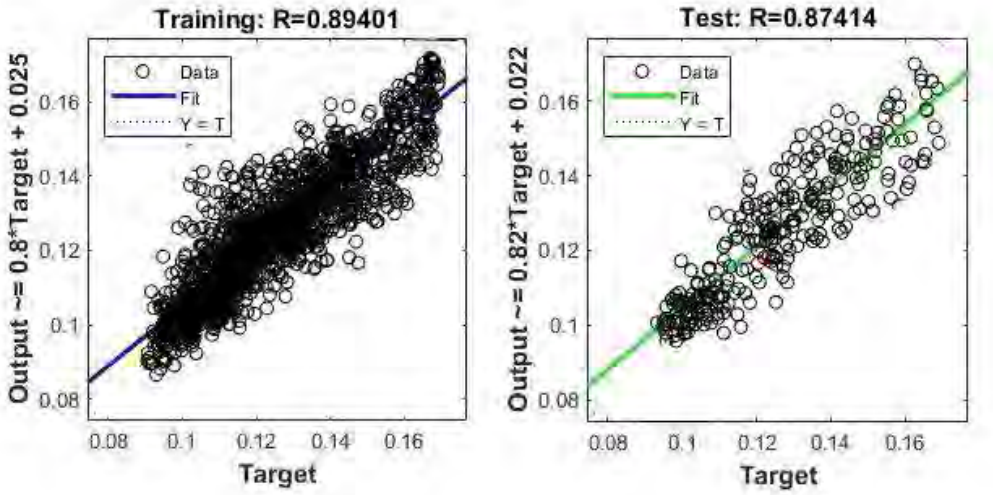

Figure 5.5: Correlation plot of training and testing dataset of Zamzama-01 well

After training and testing our network on Zamzama area, we also predict our neural network on different stratigraphic setting i.e, on Sawan area too. We kept all the input conditions similar as of Zamzama and ran the network on Sawan data. On this area the network gives us 84% correlation as shown in Figure 5.4. Figure 5.6 shows the match between measured and predicted.

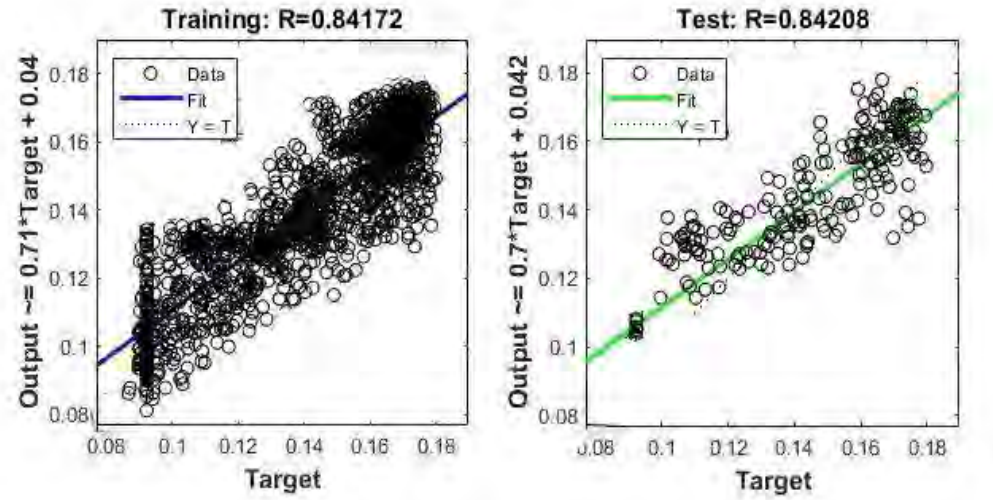

Figure 5.6: Correlation plot of training and testing dataset of Sawan-01 well

RSML

Zamzama-03 and Zamzama-05 used for reservoir characterization. But, they both don't have DT4S log in their las files. W predicted the DT4S log of both the wells using the designed neural model. The figures 5.7 and 5.8 shown the predicted DT4S log of Zamzama-03 and Zamzama-05, respectively.

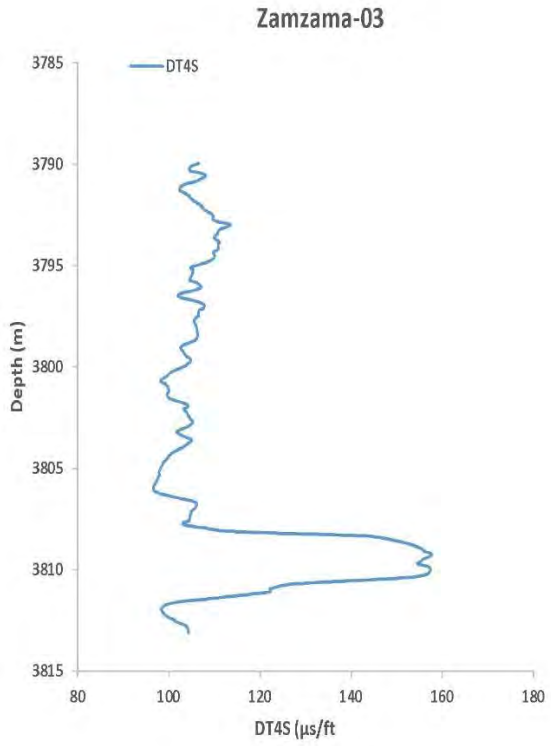

Figure 5.7: DT4S log predicted by feed-forward neural network of Zamzama-03 Well

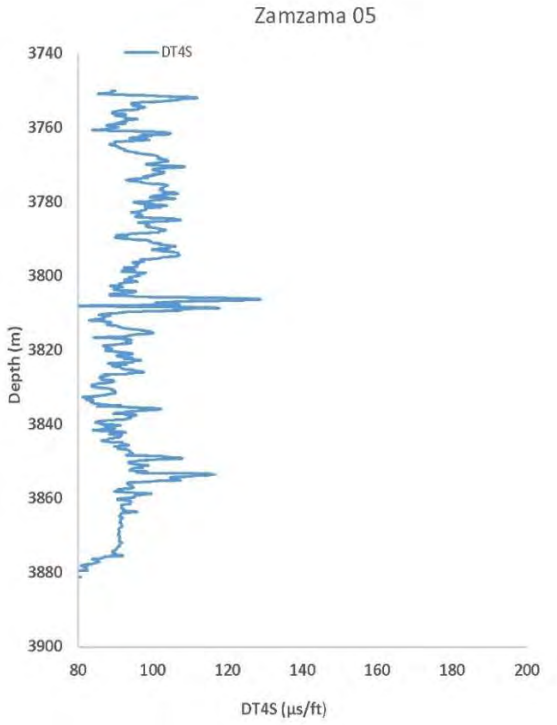

Figure 5.8: DT4S log predicted by feed-forward neural network of Zamzama-05 Well

5.5 Reservoir Characterization

Reservoir characterization is the understanding and procedures used to analyze the reservoir properties and heterogeneity (Lake & Caroll, 1986). It is a multidisciplinary, integrated task that requires skills in reservoir geology, well logging, geophysics, geostatistics, petrophysics, and reservoir engineering to create accurate pictures of petrophysical parameters required to predict reservoir performance (Srivastava, 1994). Geological models based on core, geophysical data, and wireline-log are used to create three-dimensional visualizations. By tying petrophysical characteristics to geological fabrics and employing modern geostatistical and geophysical methodologies, petrophysical properties collected from core, wireline-log, and production data are

distributed throughout the geological model. Finally, the model is put through a numerical simulator to be tested and predicted (Lucia et al., 2003).

In reservoir characterization, petrophysical analysis is particularly useful for distinguishing hydrocarbon and non-hydrocarbon bearing zones (Yuedong & Hongwei , 2007). Petrophysical analysis is utilized to translate wireline log data into reservoir parameters such as shale volume, porosity, permeability, and water and hydrocarbon saturation in the majority of cases. The ability to distinguish between hydrocarbon and non-hydrocarbon bearing zones can be greatly improved by a thorough examination of these reservoir features (Azeem et al., 2017).

Shear and compressional velocities are significant in reservoir characterization. With the help of a neural network, these velocities could be approximated. The reservoir system is an example of a physical system that exhibits both deterministic and statistical behavior (Lake & Caroll, 1986). The purpose of reservoir characterization is to create a full and detailed picture of the reservoir distribution by integrating and analyzing huge volumes of data. The elastic characteristics of the reservoir interval encountered in each well were estimated using a neural network model. The elastic characteristics (DT4S) obtained from the neural network model in the reservoir intervals are used for analysis.

Cross-plotting of parameters against each other is a useful graphical tools for identifying data clusters in targeted zones. Based on their response, these data sets can be classified into different lithologies/facies. Elastic properties (V_p/V_s ratio) enable the capacity to distinguish between different forms of lithology and payable sand in the targeted area. However, a combination of P-impedance and the V_p/V_s ratio is utilized to accurately predict lithology and fluid content (Azeem et al., 2017).

5.6 Cross Plot Analysis

This study includes Zamzama-01, 03 and 05 wells containing wireline logs (e.g., DT, RHOB, GR, SP, LLD, LLS, NPHI,). All wells have a complete set of logs, and the borehole situation in the targeted region appears to be satisfactory as well. The missing shear wave log was predicted in Zamzama 03 and 05 wells, using the above discussed neural network model in shown in Figure 5.7 and 5.8.

DRSML QAU

The elastic characteristics of the reservoir interval encountered in each well were estimated using the neural network model. The elastic properties obtained from the neural network model in the reservoir intervals are plotted against the derived petrophysical parameters from petrophysical analysis. Cross-plotting many parameters is a useful tool for visual analysis and for identifying data clusters in target zones. These data clusters can be divided into distinct lithologies/facies based on their responses. Elastic characteristics (VP/VS ratio) can distinguish between various types of lithology and payable sand in the target zone. However, a combination of P-impedance and the VP/VS ratio can be used to estimate lithology and fluid saturation with high accuracy.

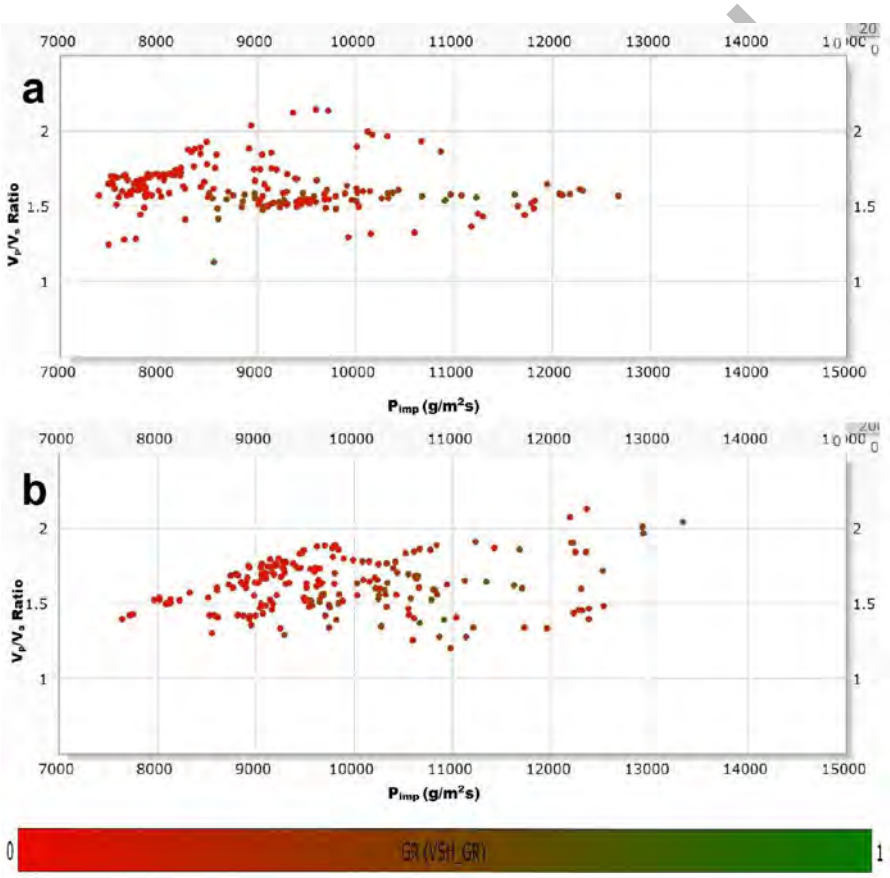

Figure 5.9: The model's effectiveness is tested by comparing measured and modelled elastic characteristics. (a) Acoustic impedance measured vs. VP/VS ratio. (b) Acoustic impedance modeled vs. VP/VS ratio. Gamma ray log colour codes the data points.

The techniques discussed previously have been applied to the wireline logs of three wells: Zamzama 01, 02, and 05. The reservoir intervals confronted in the three wells of the research region have been characterized using elastic and petrophysical parameters.

For validation of the model's performance, the measured and computed values of elastic impedance have been plotted against the V_p/V_s ratio over the whole reservoir interval (Figure 5.9). Gamma-ray log have been used to color code the data points. Figures 5.9(a) and (b) are significantly different from one another. Figure 5.9(b) shows a cross plot of modeled parameters that clearly differentiates the sand and shale facies, whereas Figure 5.9(a) shows a cross plot of measured (logs) parameters that show mixing of sand and shale facies. It's tough to distinguish lithology or fluid contents based on log data because it is influenced by a variety of factors and unpredictable circumstances. Various types of facies in all wells are distinguished based on the cross plots of Vp/Vs and acoustic impedance (Figure 5.10), keeping the model's efficiency in mind. In (Figures 5.10(a)–(c)), the low GR values and low Vp/Vs ratio indicates the clean sand lithology whereas the high GR and high Vp/Vs ratio indicates shale lithology. Gamma-ray levels in shaly sand deposits range from 80 to 120 API. If sand is gas bearing, then the acoustic impedance, and Vp/Vs ratio characteristics will be reduced but values of effective porosity will be high. The data points are color-coded using effective porosity (Figure 5.11). The gas presence has a significant impact on elastic properties, lowering acoustic impedance and the Vp/Vs ratio. The gas-bearing sediments exhibit low values of Vp/Vs and of acoustic impedance, as shown in Figures 5.11 (a), but the values of acoustic impedance are bit higher which might due to the tight reservoir, as shown in Figures 5.11 (b)–(c); further the effective porosity in these two wells (Zamzama-03 and Zamzama-05) are bit lower than the Zamzama-01 well.

If sand is gas bearing, then the acoustic impedance, and V_p/V_s ratio characteristics will be reduced but values of effective porosity will be high. The data points are color-coded using water saturation (Figure 5.12). Low values of V_p/V_s and acoustic impedance values depict gas-bearing sediments, as shown in Figures 5.12(a), but the values of acoustic impedance are bit higher which might due to the tight reservoir, as shown in Figures 5.12 (b)–(c).

DRSML QAU

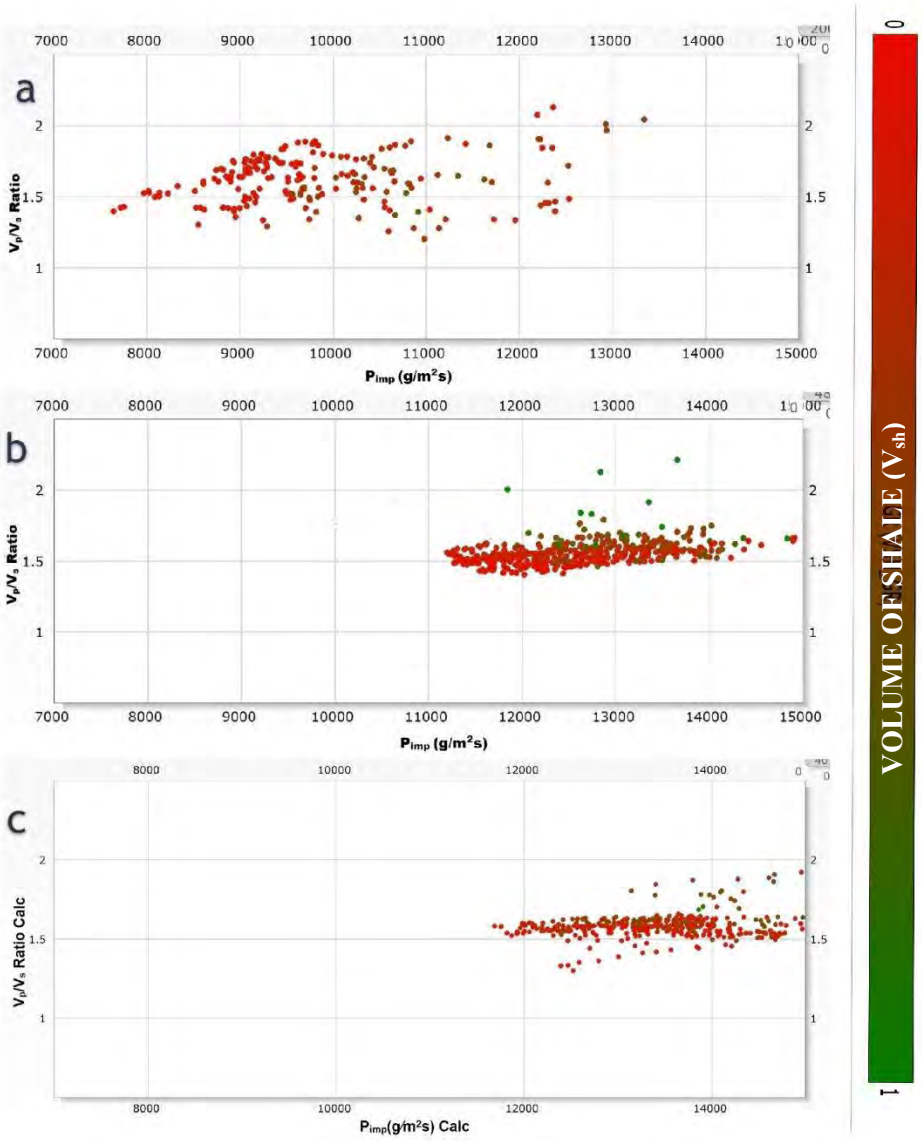

Figure 5.10: Cross plots of acoustic impedance versus V_p/V_s ratio developed using modeled elastic parameters of (a) Zamzama-01, (b) Zamzama-03, and (c) Zamzama-05 wells at various gamma ray values. Gas saturation is indicated by a data cluster with low acoustic impedance, V_p/V_s ratio, and GR values.

The data points are clearly divided into three types of clusters by the cross plots of these properties. Gas-bearing sand is represented by the cluster with low acoustic impedance, water saturation, V_p/V_s ratio, GR values and high effective porosity values. The comparison of gas-bearing sediments and gas-free sediments showed that the later has higher acoustic impedance and water saturation. The gas bearing sand and water bearing shale bodies can be identified easily with water saturation and elastic parameters through cross plots. According to the cross-plot analysis, the

calibrated model seems effective in predicting the type of rock and fluid content in the area of Zamzama gas field.

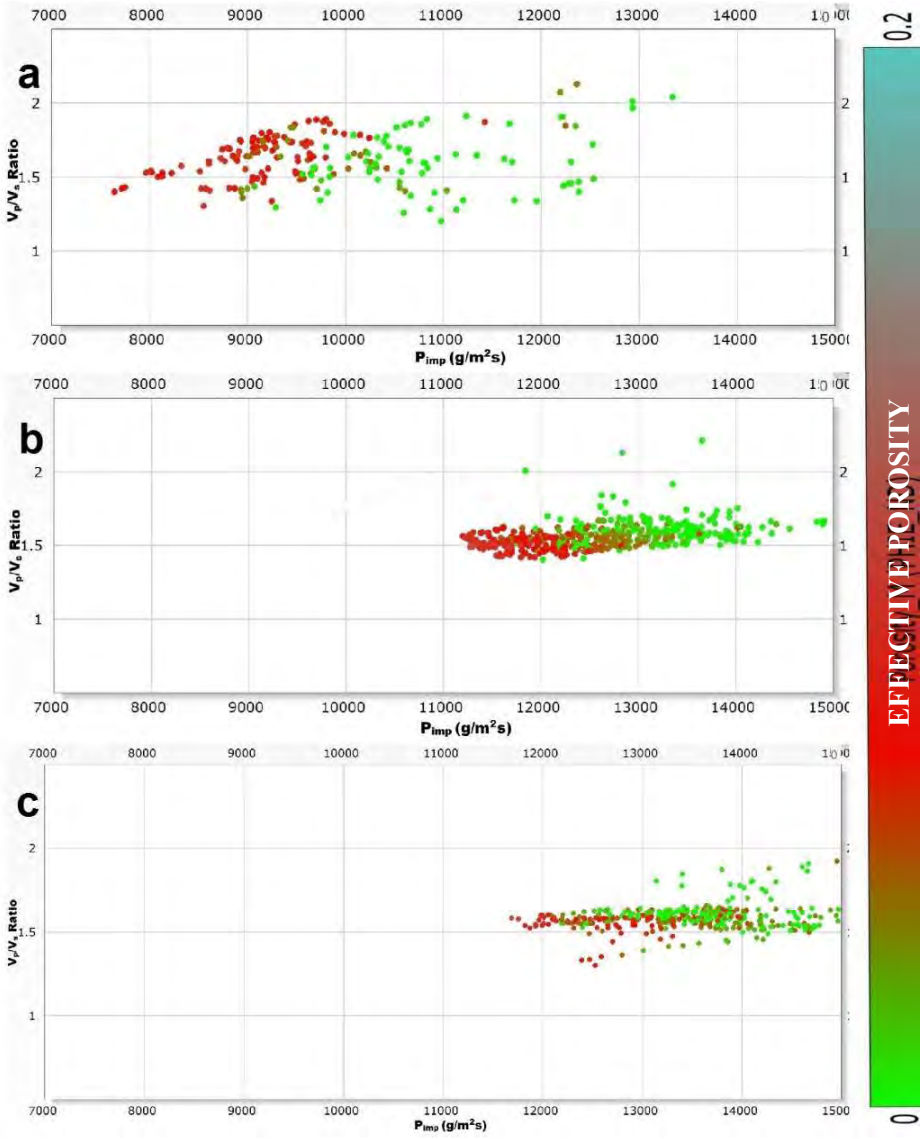

Figure 5.11: Cross plots of acoustic impedance versus Vp/Vs ratio developed using modeled elastic parameters of (a) Zamzama-01, (b) Zamzama-03, and (c) Zamzama-05 wells at various effective porosity values. Gas saturation is indicated by a data cluster with low acoustic impedance, V_p/V_s ratio, and low effective porosity values.

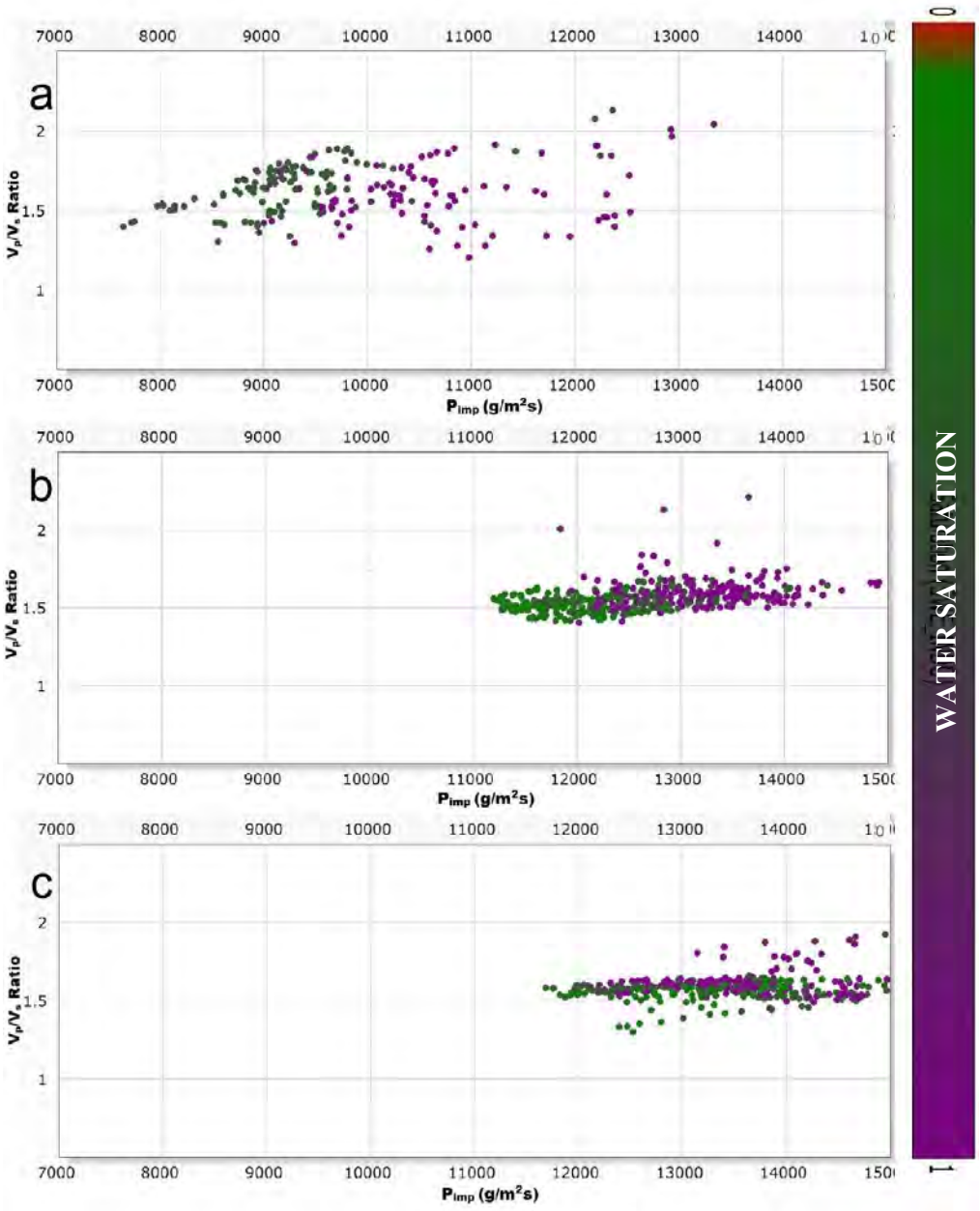

Figure 5.12: Cross plots of acoustic impedance versus Vp/Vs ratio developed using modeled elastic parameters of (a) Zamzama-01, (b) Zamzama-03, and (c) Zamzama-05 wells at various effective porosity values. Gas saturation is indicated by a data cluster with low acoustic impedance, V_p/V_s ratio, and medium water saturation values.

CHAPTER 6
WEDGE MODELING AND THIN BEDS AVO ANALYSIS

6.1 Introduction

Reservoir characterization is required for reservoir management, development, monitoring, as well as production optimization. Reservoir characterization must be dynamic in order to attain accuracy and ensure that all information available at any given time is incorporated into the reservoir model. However, to accomplish this, one must first create a primary model of the reservoir at a given moment (Aminzadeh & Dasgupta, 2013). Conventional interpretation approaches are typically employed to outline large-scale structural traps, however, they are ineffective when dealing with narrow interbedded reservoirs which are undetectable with relatively low seismic resolution (Farfour et al., 2015). Amplitude reflections of successive thin beds typically face tuning thickness difficulties due absence of high frequencies in the seismic data. As a result, amplitude anomalies are taken into account and examined using various approaches such as amplitude versus offset (AVO), amplitude versus angle (AVA), and spectral decomposition (Saeed et al., 2020).

The AVO approach uses seismic readings to obtain elastic parameters and lithological features of subsurface strata. The AVO inversion method is based on the notion that the offset variation of the P-P reflection amplitude contains all of the elastic contrast information (Buland et al., 2005). In AVO analysis, the Knott–Zoeppritz equation is used to show how transmission and reflection coefficients change with angle. AVO response is influenced by a variety of parameters, including pore fluid, lithology, offset-dependent factors, and reservoir thickness (Saeed et al., 2020).

AVO analysis becomes more difficult when dealing with a layered media with several boundaries. At zero offset, interference or tuning is determined by the dominant period of the wave, which is typically 20–100 ms. Tuning is also a function of the thin bed's interval velocity (Bakke & Ursin, 1998). The composite reflection amplitudes from a thin bed fluctuate as a measure of bed thickness for a cosine wavelet. When the layer thickness becomes equal to 1/4th of the dominant wavelength in the signal for a thin bed, inter-bedded in a homogenous background with low acoustic impedance, the constructive interference for a zero-phase wavelet is determined. Tuning thickness is another name for this (WIDESS, 1973). The influence of thin beds on seismic amplitude can be

DPSML QAU

examined using three-layer wedge modelling. Tuning thickness is the thickness of a layers where the two events become indistinguishable in the temporal domain (Bakke & Ursin, 1998).

The AVO characteristics of seismic reflections of gas sands are diverse. The AVO behaviour of a gas sand reflection is influenced by two factors: the normal incidence reflection coefficient R_0 and the contrast in Poisson's ratio at the reflector. The R_0 component is the less constrained of the two. Gas sand reflectors can be classified into three classes according to their AVO properties (Rutherford & Williams, 1989).

The goal of this research is to look at how reservoir thickness affects amplitude anomalies. The Pabstone Formation has thin strata of sandstone that operate as reservoir rocks. Due to limited seismic resolution, however, identification of these thin layers using seismic data is not possible. We have performed petrophysical-based wedge modeling and AVO analysis to solve this problem.

6.2 Wedge Modeling

According to well log examinations, the Pabstone Formation has very thin reservoir beds (Figures 4.2-4.4). Therefore, wedge modelling is utilized to assess the seismic response while taking thickness variation into account. A three-layered wedge model is built, with a reservoir layer buried between two non-reservoir layers. The elastic values required to produce the double interference wedge model are shown in Table 6.1.

Table 6.1 Elastic parameters used to develop three layer wedge model

Layers	V_p (m/s)	V_s (m/s)	Density (g/cm^3)
1	4181.705	2735.898	2.54
2	3653.367	2180.866	2.43
3	4343.928	2898.735	2.49

The following calculation is used to calculate the tuning thickness (Saeed et al., 2020).

$$z = v_i/2.8f_d \quad (6.1)$$

z= bed's tuning thickness, (λ/4)

DRSML QAU

v_i= target layer's interval velocity

f_d = dominant frequency.

The tuning thickness has been determined for dominant frequencies of 25, 30, and 35 Hz, and the results are given in Figures 6.1-6.3.

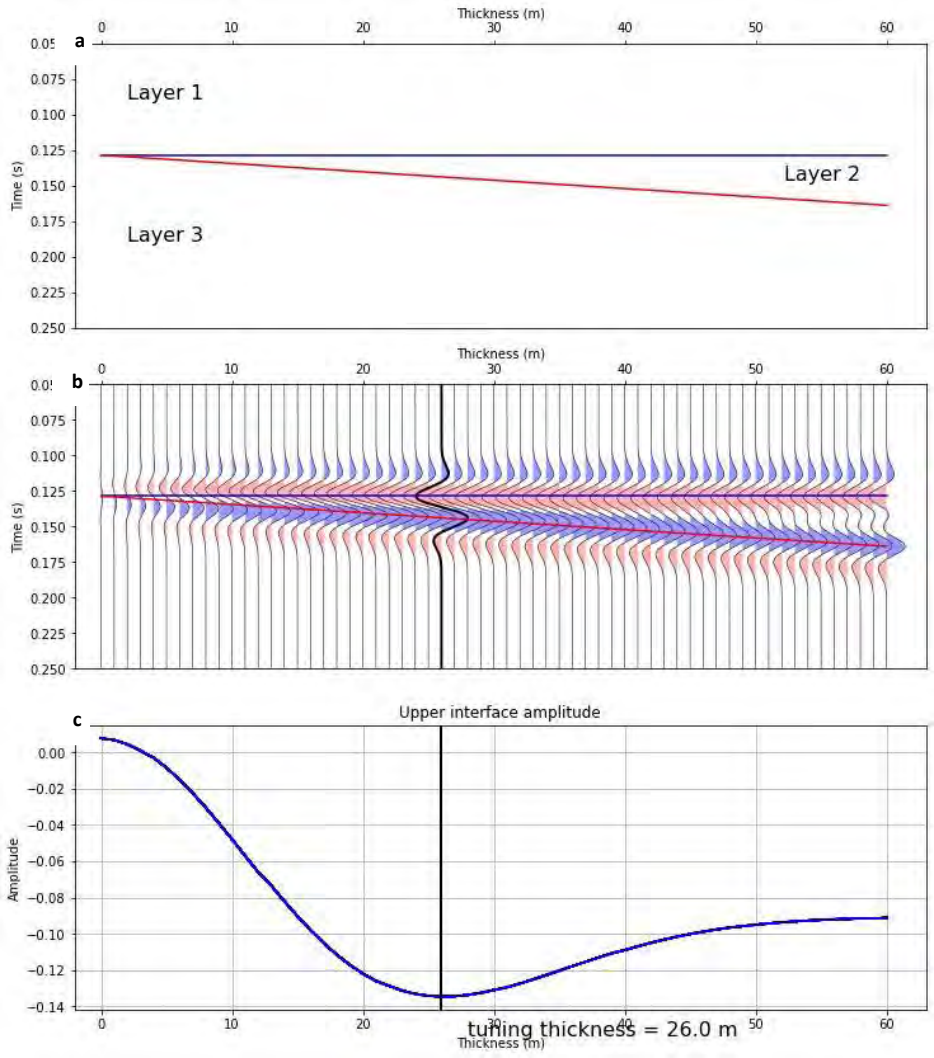

Figure 6.1: (a) Three-layer wedge model for selected interval. (b) Synthetic seismogram by using zero offset Ricker wavelet of 25 Hz frequency. (c) Amplitude of synthetic seismogram showing maximum response at 26 m thickness.

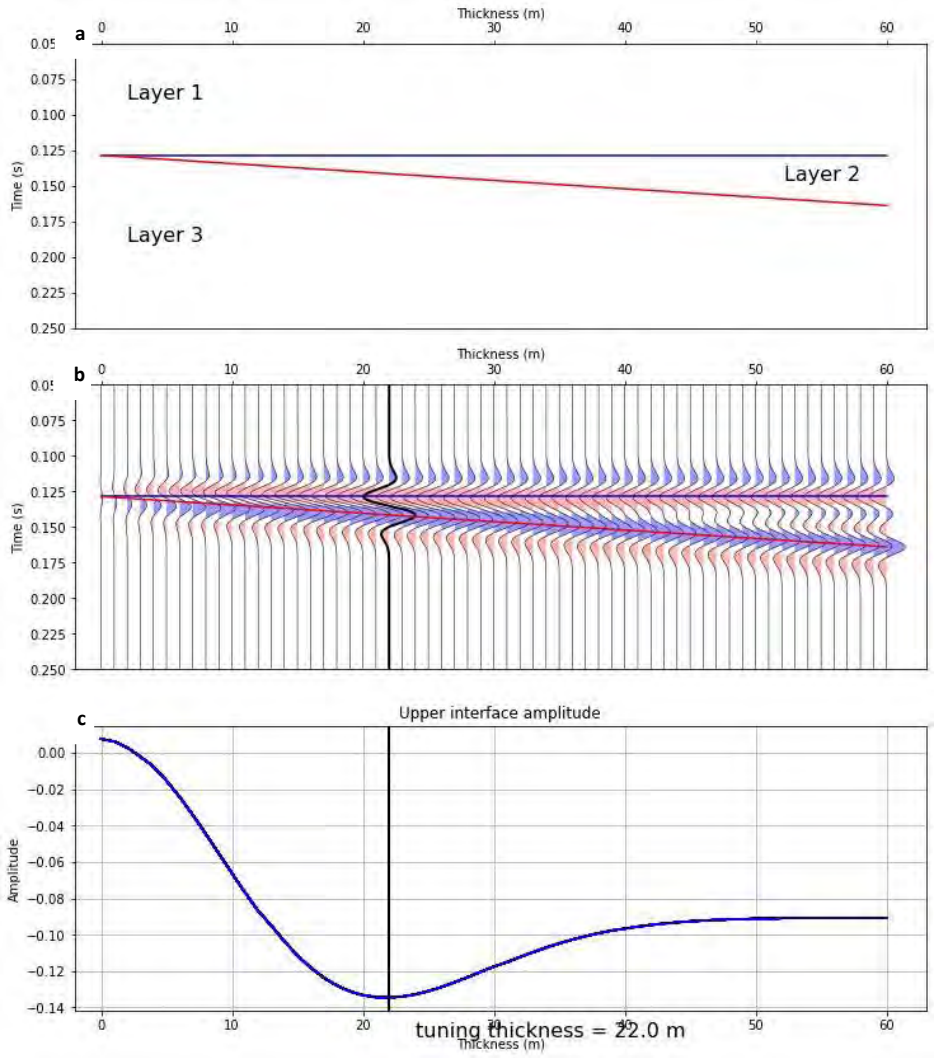

Figure 6.2: (a) Three-layer wedge model for selected interval. (b) Synthetic seismogram by using zero offset Ricker wavelet of 30 Hz frequency. (c) Amplitude of synthetic seismogram showing maximum response at 22 m thickness.

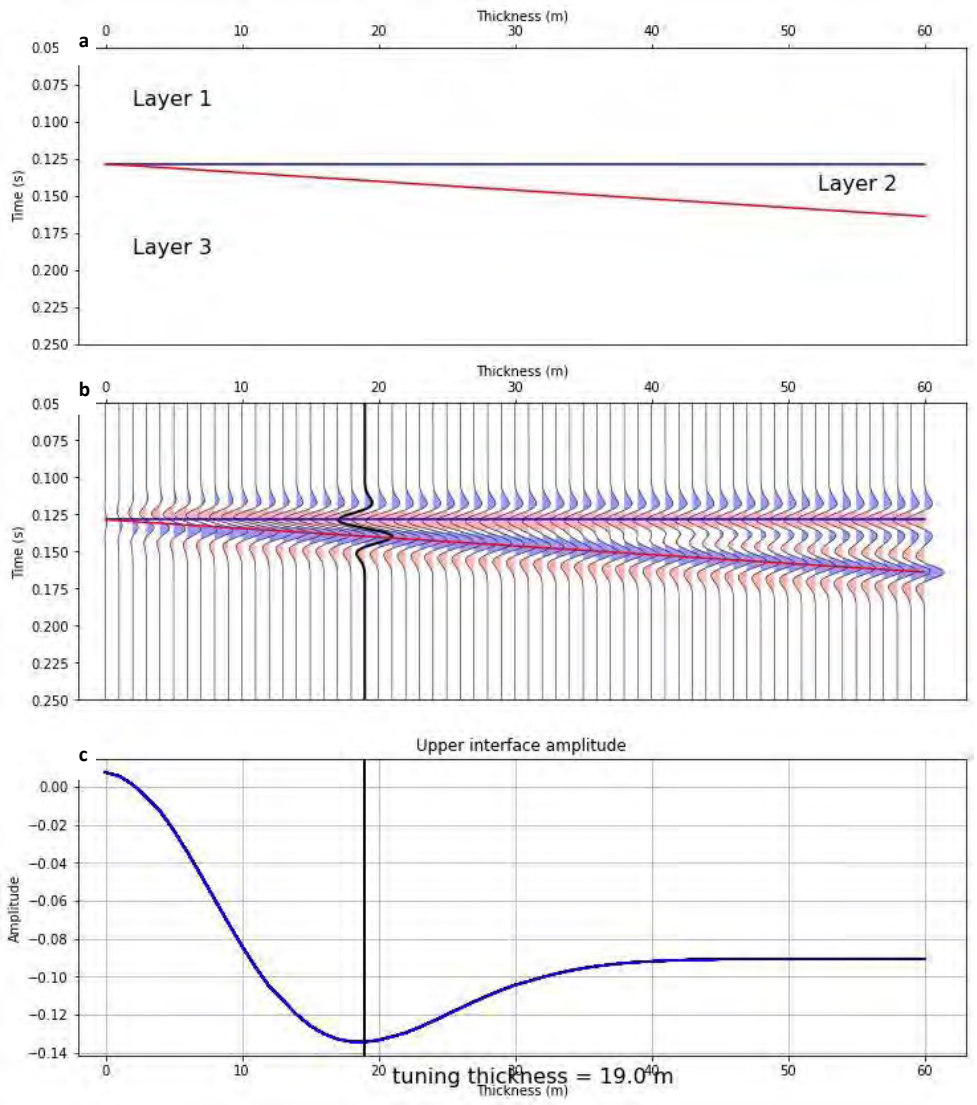

Figure 6.3: (a) Three-layer wedge model for selected interval. (b) Synthetic seismogram by using zero offset Ricker wavelet of 35 Hz frequency. (c) Amplitude of synthetic seismogram showing maximum response at 19 m thickness.

The identified reservoir interval has a 13-meter thickness that is conducive for hydrocarbon accumulation based on petrophysical study. The thickness of the reservoir zone is taken into account while creating a three-layer wedge model, with reservoir layer wedged between two non-reservoir layers.

The layer 2 pinches out towards the left and made the wedge model (Figure 6.1(a)). To create the synthetic traces, a Ricker wavelet of zero-phase having frequency of 25Hz is convolved with the reflectivity series. The horizon after the 26m are clearly distinguishable, but before 26m horizons

are can't be distinguished as shown in Figure 6.1(b). The wedge has negative impedance contracts at the top and positive impedance contrast at the bottom as evident from the wedge model. Figure 6.1(c) shows that the amplitude decreases as the thickness increases up to 26m. It is obvious from the preceding study that the seismic amplitudes peak at 26m thickness, indicating that beds having 26m thickness or greater can be easily detected on seismic section when a frequency of 25Hz is used. To investigate the variation in tuning thickness owing to changes in frequency, a similar approach is adopted for 30 and 35Hz frequencies (Figures 6.2 and 6.3). In figure 6.2 (a) the layer 2 pinches out towards the left and wedge like model is formed. Figure 6.2 (b) shows that after 22m the horizons can clearly identifiable on seismic section. The amplitude diminishes as the thickness increases up to 22m, as seen in Figure 6.2(c). The seismic amplitudes peak at 22m thickness in the study, indicating that beds with a thickness of 22m or larger can be easily recognized on seismic sections when a frequency of 30Hz is utilized. Layer 2 pinches out to the left in figure 6.3 (a), forming a wedge-like shape. The horizons can be easily identified on seismic section after 19m, as shown in Figure 6.3 (b). As the thickness grows up to 19m, the amplitude decreases, as seen in Figure 6.3. (c). When a frequency of 35Hz is used, the seismic amplitudes peak at 19m thickness in the study, showing that beds with a thickness of 19m or larger can be easily identified on seismic sections. Wedge model results show that reservoir layers with thicknesses of 22m and 19m may be easily resolved using seismic data at 30Hz and 35Hz frequencies, respectively.

DRSML OAU

6.3 AVO Analysis

The foundation of AVO theory is the Zoeppritz equation, which gives the wave reflection and transmission coefficients as a function of the angle of incidence and elastic factors. Shifts in elastic properties can be used to infer litho-fluid changes from one layer to the next. Precise Zoeppritz equation is used to study the variation in reflection coefficients with respect to incidence angle at the top and bottom of the target range. The actual Zoeppritz equation that was employed is given by (Zoeppritz, 1919) as follows:

$$\begin{bmatrix} R_p \\ R_s \\ T_p \\ T_s \end{bmatrix} = \begin{bmatrix} -sin\theta_1 & cos\varphi_1 & sin\theta_2 & cos\varphi_2 \\ cos\theta_1 & sin\ _1 & cos\theta_2 & -sin\varphi_2 \\ sin2\theta_1 & -\frac{V_{p1}}{V_{s1}}cos2\varphi_1 & \frac{\rho_2 V_{s2}^2 V_{p1}}{\rho_1 V_{s1}^2 V_{p2}}sin2\theta_2 & \frac{\rho_2 V_{s2}^2 V_{p1}}{\rho_1 V_{s1}^2 V_{p2}}cos2\varphi_2 \\ cos2\theta_1 & -\frac{V_{p1}}{V_{s1}}sin2\varphi_1 & \frac{\rho_2 V_{p2}}{\rho_1 V_{p1}}cos2\varphi_2 & -\frac{\rho_2 V_{p2}}{\rho_1 V_{p1}}sin2\varphi_2 \end{bmatrix} \begin{bmatrix} sin\theta_1 \\ cos\theta_1 \\ sin2\theta_1 \\ cos2\varphi_1 \end{bmatrix} \quad (6.2)$$

R_p= P-wave reflection coefficient

R_s= S-wave reflection coefficient

T_p= P-wave transmitted amplitude

T_s= S-wave transmitted amplitude

θ_1, θ_2= Reflection angels

φ_1, φ_2= Transmission angles

V_{p1}, V_{s1}= P and S-wave velocity of upper half space

V_{p2}, V_{s2}= P and S-wave velocity of lower half space

ρ_1, ρ_2= Densities of upper half space

The objective is to determine thickness differences and their impact on AVO response. To study the effect of thickness, the reflection coefficients generated from the Zoeppritz equation are convolved with the Ricker (source) wavelet. Because the thickness of the layer affects the travel time values, the two-way travel time values were used to derive the convolving coefficients. Finally, the Shuey's approximation was used to get the intercept and gradient values at various thicknesses. The influence of thickness on AVO qualities was then investigated by cross-plotting these attributes. The Shuey's equation that was employed is given by (Shuey, 1985) as follows:

$$R(\theta) \approx R(O) + Bsin^2\theta + C(sin^2\theta tan^2\theta) \quad (6.3)$$

$$R(O) = \frac{1}{2}\left(\frac{\Delta V_P}{V_P} + \frac{\Delta \rho}{\rho}\right) \quad (6.4)$$

$$B = -2\left(1 - \frac{\sigma}{1-\sigma}\right)R(O) - \frac{1}{2}\frac{1-3\sigma}{1-\sigma}\frac{\Delta V_p}{V_p} + \frac{\Delta \sigma}{(1-\sigma)^2} \quad (6.5)$$

$$C = \frac{1}{2}\frac{\Delta V_p}{V_p} \quad (6.6)$$

V_p, V_s = Contrast of P and S-wave velocities, respectively.

DRSML QAU

V_p, V_s = Average of P and S-wave velocities, respectively.

$\Delta\sigma, \Delta\rho$= Contrast of Poisson's Ration and Density, respectively.

σ, ρ = Average of Poisson's Ration and Density, respectively.

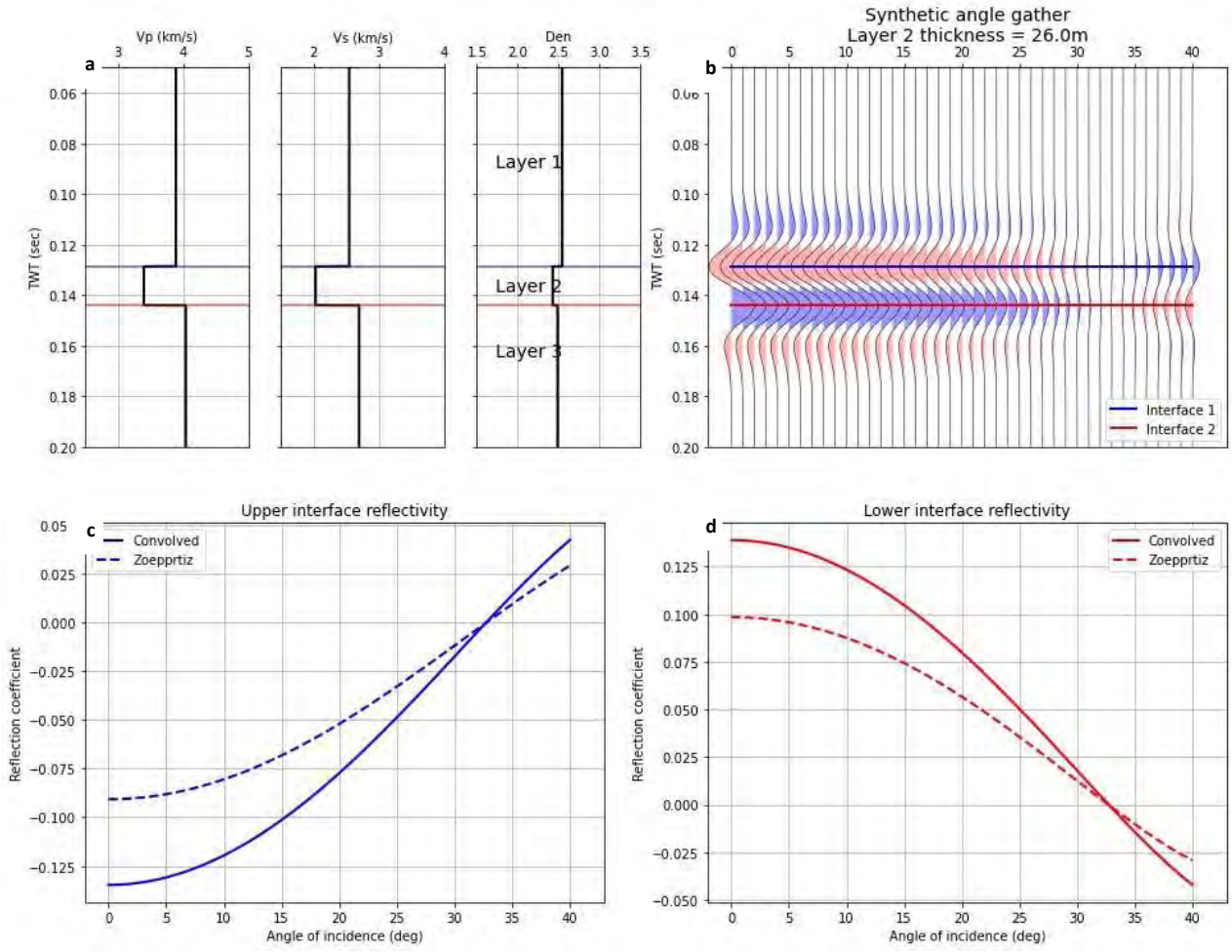

Figure 6.4: (a) Reflectivity response of elastic parameters for selected interval. (b) Synthetic angle gathers considering the 26 m bed thickness. (c) Angle-dependent reflectivities (amplitude) estimated with convolved and standard Zoeppritz equations of the upper interface. (d) Angle-dependent reflectivities (amplitude) estimated with convolved and standard Zoeppritz equations of the lower interface.

The reflection coefficients at the normal angle of incidence, also known as the AVO intercept, are represented as $R(O)$. The AVO gradient is represented by B, and it explains the fluctuation in reflection amplitudes at a mid-angle of incidence. The third term C, stands for curvature, and it describes how reflection coefficients behave at large angles of incidence, sometimes near the

critical angle. Shuey's equation can be reduced to a two-term equation if the angle of incidence is less than 30 degrees as:

$$R(\theta) \approx R(O) + Bs \quad ^2\theta \qquad (6.7)$$

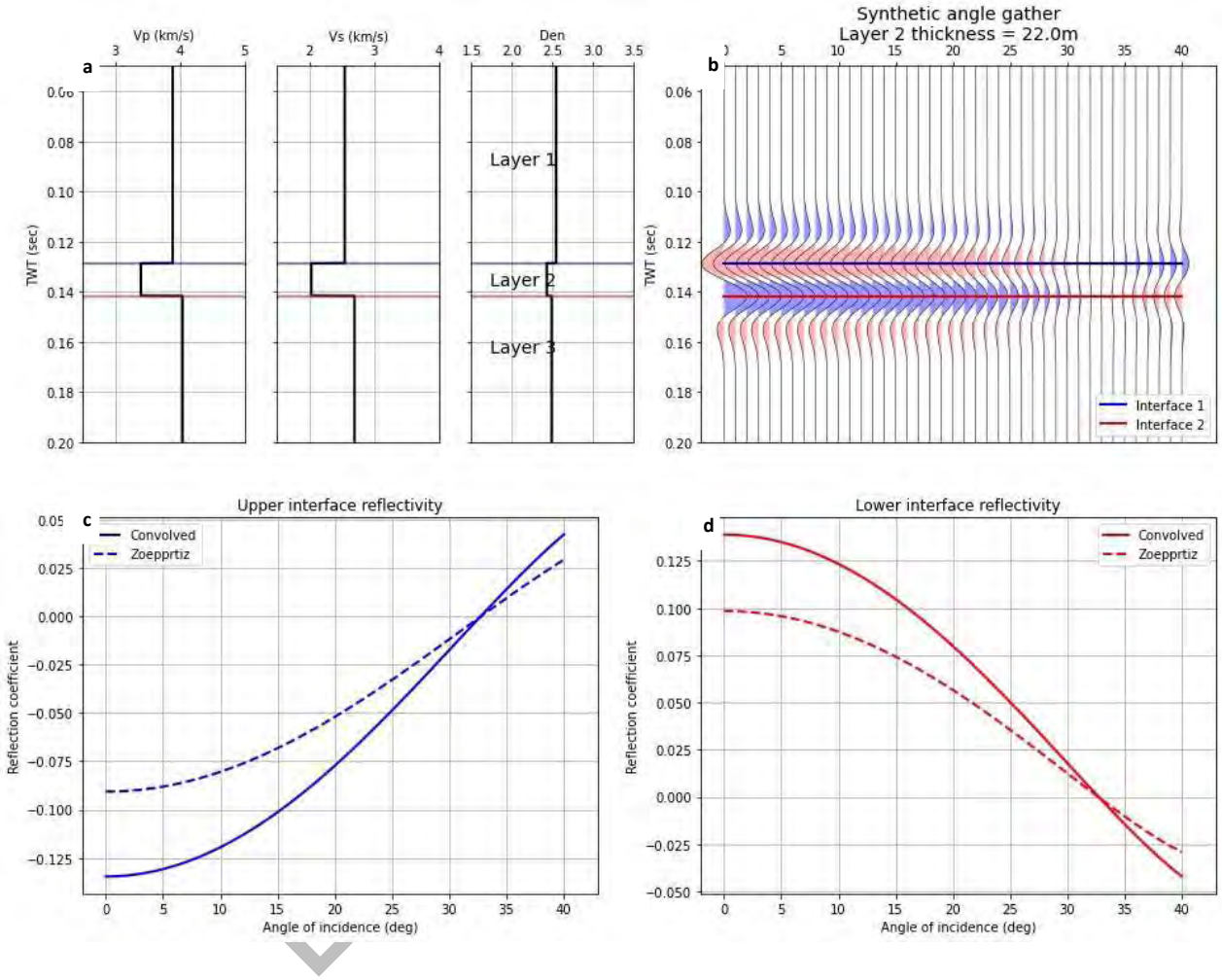

Figure 6.5: (a) Reflectivity response of elastic parameters for selected interval. (b) Synthetic angle gathers considering the 22 m bed thickness. (c) Angle-dependent reflectivities (amplitude) estimated with convolved and standard Zoeppritz equations of the upper interface. (d) Angle-dependent reflectivities (amplitude) estimated with convolved and standard Zoeppritz equations of the lower interface.

At zero offset, the synthetic gathers were observed. Synthetic angle gathers are investigated to gain understanding of thin bed adjustment and their influence on angle-dependent reflectivity. Angle-dependent reflectivity (amplitudes) over the top and bottom interfaces (Figures 6.4a & b) are calculated using precise Zoeppritz equations with a bed thickness of 26 m (Figures 6.4c & d). The

convolved amplitudes have been addressed to get an idea of reflectivity response for layers which are very thin.

Figure 6.4c (upper interface) indicates with the increase in the angle of incidence, values of reflection coefficient of convolved and zoeppritz increases. The value of convolved amplitudes, on the other hand, increases more quickly than the Zoeppritz amplitudes crossing its reflectivities at a 32-degree angle. The convolved amplitudes grow smaller than the Zoeppritz reflectivity after that angle, which could suggest destructive interface. The reflectivity at the lower interface, on the other hand, are the polar opposite of those along the top interface (Figure 6.4d). With increasing angle of incidence, the gap between these amplitude curves narrows as well; yet, these two reflectivity curves (convolved and Zoeppritz) cross at angle 32.

Similarly, we conducted AVO analyses for 22m and 19m thicknesses, using 30Hz and 35Hz frequencies respectively. Figures 6.5 and 6.6 depict the acquired results. It is obvious from these results (Figures 6.5 & 6.6) that the reflectivity responses obtained along the top and bottom interfaces are identical to those reported for 26 m thickness at a frequency of 25 Hz (Figure 6.4). Seismic data with prominent frequencies of 25 Hz, 30 Hz, and 35 Hz can be used to identify zones with thicknesses of 19m, 22m, and 26m respectively. AVO modelling gives Class IV AVO response from the top layer of gas-bearing sand.

DRSML QAU

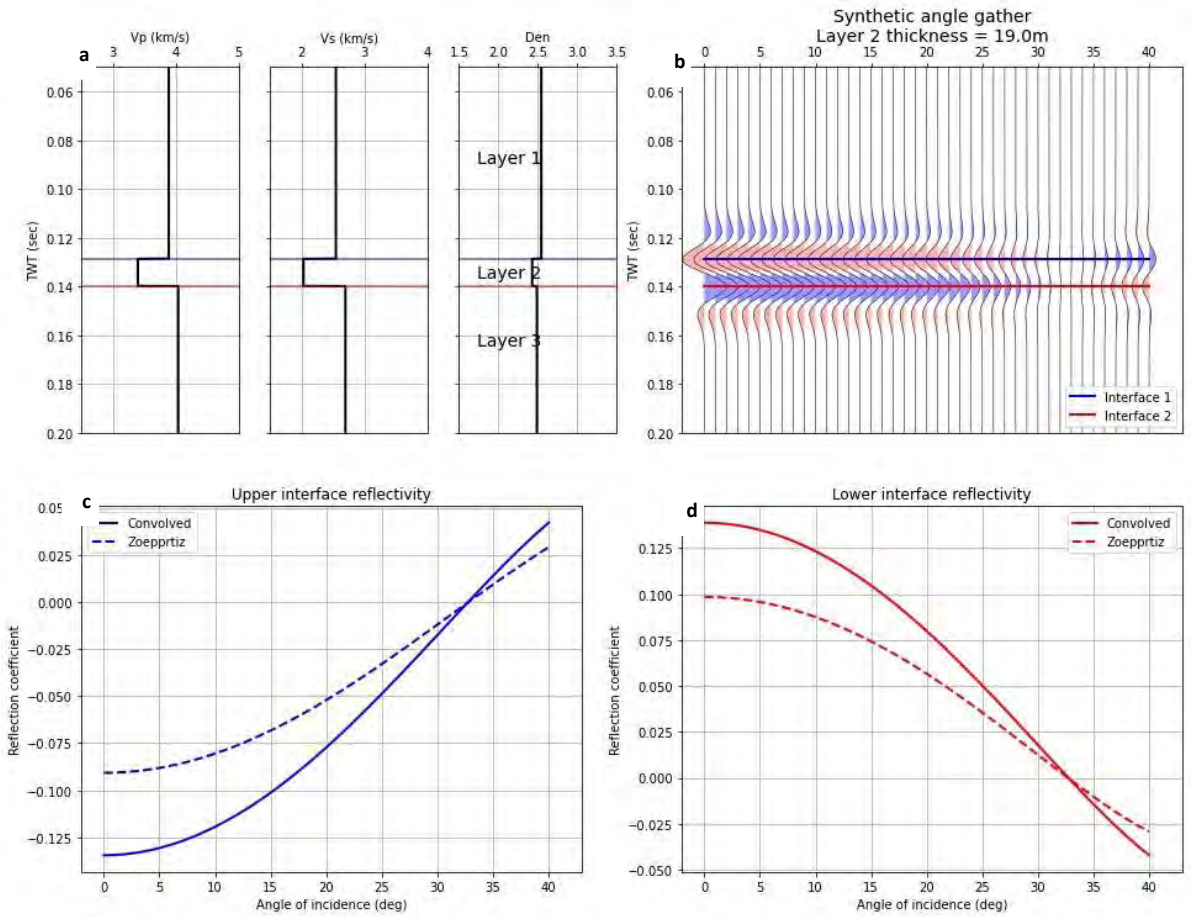

Figure 6.6: (a) Reflectivity response of elastic parameters for selected interval. (b) Synthetic angle gathers considering the 19 m bed thickness. (c) Angle-dependent reflectivities (amplitude) estimated with convolved and standard Zoeppritz equations of the upper interface. (d) Angle-dependent reflectivities (amplitude) estimated with convolved and standard Zoeppritz equations of the lower interface

DRAFT

RESULTS AND CONCLUSIONS

This study analyzes the Pabstone formation, in Zamzama area, Central Indus Basin, Pakistan. 3D seismic data and well log data of Zamzama-01, 03, and 05 was used for interpretational purpose. 3D seismic interpretations indicate that the Zamzama field, which is extensively scattered, contains thrusted anticlinal structure.

The depth of resource formation is of particular significance since it has a direct impact on the economic aspect in analysis. Petrophysical analysis reveals, Pabstone act as reservoir rock in Zamzama gas field. It has many thin beds of sands ranging from 8 to 13m that act as economical reservoirs. To characterize this reservoir, DT4S log is necessary. Feed forward neural network is designed to estimate and predict the DT4S log using well log data as input. Input for neural network model was selected using feature importance. 87% matching was observed in estimation of DT4S log in Zamzama area. Same neurak network model was applied on Sawan area, 84% matching was also observed in this area. After calculating DT4S log in Zamzama well-01, 03 and 05, cross plot analysis was done using calculated elastic parameter, to distinguish the reservoir and non-reservoir zone.

Thin bed wedge modeling and AVO analysis was carried out to resolve the thin beds of reservoir. Different dominant frequencies are used for this purpose. Dominant frequency of given seismic data was 25 Hz which resolved the beds of thickness more than 26m, whereas 30 Hz and 35 Hz resolves the beds of thickness more than 22m and 19m, respectively.

Conclusions of the study are as follows:

- Three dimensional seismic interpretations reveal that thrusted anticlinal structure is present in the Zamzama field
- Petrophysical analysis shows one prospect zone in Zamzama-01, in which shale volume is 10%, effective porosity is 11% and hydrocarbon saturation is 75%.
- According to a petrophysical analysis, one prospective zone in Zamzama-03 contains 15% shale volume, 9% effective porosity, and 70% hydrocarbon saturation.
- One potential zone in Zamzama-05, according to a petrophysical analysis, comprises 12% shale volume, 9% effective porosity, and 68% hydrocarbon saturation.

DRSML QAU

- Feed-forward neural network give us more than 80% accuracy for calculating DT4S in Zamzama as well as in Sawan field.
- Cross plot analysis was also done using calculated elastic parameters to clearly distinguish between reservoir and non-reservoir zone.
- Thin beds were identified with the help of wedge modeling using 25 Hz, 30 Hz, and 35 Hz, which resolved 26m, 22m, and 19m thin beds, respectively. AVO modeling gave Class IV AVO response from the top layer of gas-bearing sand.

Recommendations

Thin beds reservoirs ranging of thickness 8-15m were observed which are not resolvable with the help of conventional AVO technique. As we have thin beds reservoir throughout the Pabstone in Zamzama field, it is necessary to resolve these beds. These thin beds can be resolved with the help of stochastic AVO modeling.

DRSML QAU

References

Arshad, K., Imran, M., & Iqbal, M. (2013). Hydrocarbon Prospectivity And Risk Analysis Of An Under-Explored Western Kirthar Fold Belt Of Pakistan. *Offshore Mediterranean Conference and Exhibition*.

Abdelwahhab, M., & Raef, A. (2020). Integrated reservoir and basin modeling in understanding the petroleum system and evaluating prospects: The Cenomanian reservoir, Bahariya Formation, at Falak Field, Shushan Basin, Western Desert, Egypt. *Journal of Petroleum Science and Engineering*, 107023.

Akhundi, H., Ghafoori, M., Reza, G., & Lashkaripour. (2014). Prediction of Shear Wave Velocity Using Artificial Neural Network Technique, Multiple Regression and Petrophysical Data: A Case Study in Asmari Reservoir (SW Iran). *Scientific Research, 4*, 11.

Al-Anazi, A., & Gates, I. (2010). Support vector regression for porosity prediction in a heterogeneous reservoir: A comparative study. *Computers & Geosciences*, 1494-1503.

Alsadi, H. (2017). *Seismic Hydrocarbon Exploration.* Springer.

Aminzadeh, F., & Dasgupta, S. (2013). Reservoir Characterization. *Geophysics for Petroleum Engineers*.

An integrated petrophysical and rock physics analysis to improve reservoir characterization of. (n.d.). *GeophysicsE*.

Asim, S., Khan, N., Qureshi, S., Hussain, F., & Bablani, S. (2014). Study of a Stratigraphic Trap of Paleocene/Late Cretaceous Age with the Help of Seismic Data in Sulaiman Foredeep and Kirthar Foredeep Area (Central & Southern Indus Basin, Pakistan). *International Journal of Geosciences*.

Asquith, G., & Krygowski, D. (2006). *Basic Well Log Analysis.* AAPG.

Azeem, T., Chun, W., Lisa, M., Khalid, P., Qing, L., Ehsan, M., . . . Wei, X. (2017). An integrated petrophysical and rock physics analysis to improve reservoir characterization of. *Geophysics Engineering*, 212.

Bakke, N., & Ursin, B. (1998). Thin Bed AVO Effects. *Geophysical Prospecting*, 571-587.

Ball, N., & Brunner, R. (2010). Data mining and machine learning in astronomy. *International Journal of Modern Physics*, 1049-1106.

Bjørlykke, K. (2014). Relationships between depositional environments, burial history and rock properties. Some principal aspects of diagenetic process in sedimentary basins. *Sedimentary Geology*, 1-14.

Brownlee , J. (2020). How to Calculate Feature Importance With Python. *Machine Learning Mastery*.

Buland, A., Landroø, M., Sollie, R., Andersen, M., & Dahl, T. (2005). Lithology identification by AVO inversion. *Society of Exploration Geophysicists*, 1115-1118.

Buryakovsky, L., Chilingar, G., Rieke, H., & Shin, S. (2012). *Fundamentals of the Petrophysics of Oil and Gas Reservoirs.* New Jersey: Wiley.

Carter, M., & Gregorich, E. (2007). *Soil Sampling and Methods of Analysis.* Boca Raton: Canadian Society of Soil Sciences.

DRSML-QAU

Castagna, J., Batzle, M., & Eastwood, R. (1985). Relationships between compressional-wave and shear wave velocities in clastic silicate rocks. *Geophysics*, 571-581.

Coffeen, J. (1986). *Seismic exploration fundamentals.* Tulsa, Okla: PPC.

D.Sanger, T. (1989). Optimal unsupervised learning in a single-layer linear feedforward neural network. *Neural Networks*, 459-473.

Das, B., Chatterjee, R., Singha, D., & Kumar , R. (2017). Post-stack seismic inversion and attribute analysis in shallow offshore of Krishna-Godavari basin, India. *Journal of the Geological Society of India*, 32–40.

Fanchi, J. (2005). *Principles of Applied Reservoir Simulation.* U.S.A: Gulf Professional Plubshier.

Fang, Z., Wang, Y., Peng, L., & Hong, H. (2020). Integration of convolutional neural network and conventional machine learning classifiers for landslide susceptibility mapping. *Computers & Geosciences*, 104470.

Faraklioti, M., & Petrou, M. (2003). Horizon Picking in 3D Seismic Images. *Springer*, 216-222.

Farfour, M., Yoon, W., & Kim, J. (2015). Seismic attributes and acoustic impedance inversion in interpretation of complex hydrocarbon reservoirs. *Journal of Applied Geophysics*, 68-80.

Fu, L.-Y. (2003). An Information Integrated Approach for Reservoir Characterization. *Springer*, 157-178.

Fu, L.-Y. (2001). Caianiello neural network method for geophysical inverse problems. *Handbook of Geophysical Exploration: Seismic Exploration*, 187-215.

Ghorbani, A., Jafarian, Y., & Maghsoudi, M. (2012). Estimating shear wave velocity of soil deposits using polynomial neural networks: Application to liquefaction. *Computers & Geosciences*, 86-94.

Gunderson, K., & Huffman, K. (2018). Teaching Structural Geology Techniques for Applied Subsurface Interpretation and Characterization. *Teaching Methodologies in Structural Geology and Tectonics*, 123-157.

Hampson, D., Schuelke, J., & Quirein, J. (2001). Use of multiattribute transforms to predict log properties from seismic data. *Geophysics, 66*, 220-236.

Hossain, T., Watada, J., Aziz, I., & Hermana, M. (2020). Machine Learning in Electrofacies Classification and Subsurface Lithology Interpretation: A Rough Set Theory Approach. *Applied Sciences*.

Hussain, M., Ahmed, N., Chun, W., Khalid, P., Mahmood, A., Ahmad, S., & Rasool, U. (2017). Reservoir Characterization of Basal Sand Zone of Lower Goru Formation by Petrophysical Studies of Geophysical Logs. *GEOLOGICAL SOCIETY OF INDIA*, 331-338.

Ilonen, J., Kamarainen, J.-K., & Lampinen , J. (2003). Differential Evolution Training Algorithm for Feed-Forward Neural Networks. *Neural Processing Letters*, 93–105.

Iqbal, M., Rahman, S., Nabil, S., & Chowdhury, I. (2012). Knowledge based decision tree construction with feature importance domain knowledge. *IEEE*.

Jackson, M., Jellis, R., Hill, R., Roberson, P., Woodall, M., Wormald, G., & Jafri, N. (2004). Zamzama Gas Field - Balancing Risk and Value. *SPE Asia Pacific Oil and Gas Conference and Exhibition*.

DRSML-OAU

Kamel, M., & Mabrouk, W. (2002). An equation for estimating water saturation in clean formations utilizing resistivity and sonic logs: theory and application. *Journal of Petroleum Science and Engineering*, 159-168.

Kazmi,, A., & Jan, , Q. (1997). *Geology and tectonics of Pakistan.* Karachi: Graphic.

Knackstedt, M., Jaime, P., Butcher, A., Botha, P., Middleton, J., & Sok, R. (2010). Integrating Reservoir Characterization: 3D Dynamic, Petrophysical and Geological Description of Reservoir Facies. *SPE Asia Pacific Oil and Gas Conference and Exhibition*, SPE-133981-MS.

Konate, A. A., Pan, H., Khan, N., & Yang, J. H. (2014). Generalized regression and feed-forward back propagation neural networks in modelling porosity from geophysical well logs. *EXPLORATION GEOPHYSICS*, EXPLORATION GEOPHYSICS.

Lake, L., & Caroll, Jr, H. (1986). *Reservoir Characterization.* Academic Press.

Larsen, R., Brekke, H., Larsen, B., & Talleraas, E. (1992). *Structural and Tectonic Modelling and its Application to Petroleum Geology.* Norway: Norwegian Petroleum Society.

Latimer, R. B., Davidson, R., & Riel, P. v. (2000). An interpreter's guide to understanding and working with seismic-derived acoustic impedance data. *The League Edge, 19*, 242-256.

Lucia, F., Kerans, C., & Jennings, Jr., J. (2003). Carbonate Reservoir Characterization. *Journal of etroleum Technology*, 70-72.

M.H, R. (1986). *The geological interpretation of well logs.* U.S.A.

Mahmood, M., & Ahmad, Z. (2017). Application of Multi-Layer Feed Forward Neural Network (MLFNN) for the Prediction of Porosity: A Case Study from Lower Indus Basin, Pakistan. *The Nucleus*, 10-15.

Mitchum, R., & Vail, P. (1997). *Seismic Stratigraphy--Applications to Hydrocarbon Exploration.* AAPG.

Monreal, F., Villar, H., Baudino, R., Delpino, D., & Zencich, S. (2009). Modeling an atypical petroleum system: A case study of hydrocarbon generation, migration and accumulation related to igneous intrusions in the Neuquen Basin, Argentina. *Elsevier*, 590-605.

Mughal , M., & Akhter, G. (2021). Predicting the gas resource potential in reservoir C-sand interval of Lower Goru Formation, Middle Indus Basin, Pakistan. *Open Geosciences*.

Noori, R., Karbassi, A., Moghaddamnia, A., Han, D., Ashtiani, M., Farokhnia, A., & Gousheh, M. (2011). Assessment of input variables determination on the SVM model performance using PCA, Gamma test, and forward selection techniques for monthly stream flow prediction. *Journal of Hydrology*, 177-189.

Onajite , E. (2013). *Seismic data analysis techniques in hydrocarbon exploration.* Amsterdam: Elsevier.

Peterson, R., Fillippone, W., & Coker, F. (2002). THE SYNTHESIS OF SEISMOGRAMS FROM WELL LOG DATA. *GEOPHYSICS*, 503-687.

Polo, M., Dahlke, T., Frogner, C., Zhang, C., Poggio, T., & Hohl, D. (2017). Automated fault detection without seismic processing. *The Leading Edge*, 194–280.

Qadri, I. (1995). *Petroleum Geology of Pakistan.* Ferozson (Pvt) Ltd.

DRSML QAU

Qureshi, M., Ghazi, S., Riaz, M., & Ahmad, S. (2020). Geo-seismic model for petroleum plays an assessment of the Zamzama area, Southern Indus Basin, Pakistan. *Springer*, 33-44.

Raeesi, M., Moradzadeh, A., Ardejani, F., & Rahimi, M. (2012). Classification and identification of hydrocarbon reservoir lithofacies and their heterogeneity using seismic attributes, logs data and artificial neural networks. *Journal of Petroleum Science and Engineering*, 151-165.

Rajbahadur, G., Wang, S., Ansaldi, G., Kamei, Y., & Hassan, A. (2021). The impact of feature importance methods on the interpretation of defect classifiers. *IEEE*.

Raza, M., Khan, F., Khan, M., Riaz, M., & Khan, U. (2020). Reservoir Characterization of the B-Interval of Lower Goru Formation, Miano 9 and 10, Miano area, Lower Indus Basin, Pakistan. *IIETA*.

Rider, M. (1990). Gamma-ray log shape used as a facies indicator: critical analysis of an oversimplified methodology. *Geological Society*, 27-37.

Ronaghan, S. (2018). The Mathematics of Decision Trees, Random Forest and Feature Importance in Scikit-learn and Spark. *Science Direct*.

Russell, B., Lines, L., & Hampson, D. (2003). Application of the radial basis function neural network to the prediction of log properties from seismic attributes. *Exploration Geophysics*, 15 - 23.

Rutherford, S., & Williams, R. (1989). Amplitude-versus-offset variations in gas sands. *GEOPHYSICS*, 680-789.

Saeed, W., Zhang, H., Guo, Q., Ali, A., Azeem, T., Toqeer, M., . . . Hussain, M. (2020). An integrated petrophysical-based wedge modeling and thin bed AVO analysis for improved reservoir characterization of Zhujiang Formation, Huizhou sub-basin, China: A case study. *Open Geosciences*.

Sheriff, R. (1976). Inferring Stratigraphy from Seismic Data1. *AAPG Bulletin*, 528–542.

Sheriff, R. (1999). *Encyclopedia Dictionary of Exploration Geophysics.* Tulsa, Oklahoma: Society of Exploration geophysists.

Shuey, R. (1985). A simplification of the Zoeppritz equations. *GEOPHYSICS*.

Singh, S., & Kanli, A. (2016). Estimating shear wave velocities in oil fields: a neural network approach. *Geosciences*, 221-228.

Srivastava, R. (1994). *Stochastic Modeling and Geostatistics.* AAPG.

Sun, H., & Hu, X. (2017). Attribute selection for decision tree learning with class constraint. *Chemometrics and Intelligent Laboratory Systems*, 16-23.

Suzuki, K. (2011). ARTIFICIAL NEURAL NETWORKS METHODOLOGICAL ADVANCES AND BIOMEDICAL APPLICATIONS. *Academia*.

Svozil, D., Kvasnicka, V., & Pospichal, J. (1997). Introduction to multi-layer feed-forward neural networks. *Chemometrics and Intelligent Laboratory Systems*, 43-62.

Tang, P., & Peng, Y. (2017). Exploiting distinctive topological constraint of local feature matching for logo image recognition. *Neurocomputing*, 113-122.

DRSML-QAU

Tiab, D., & Donaldson, E. (2015). *Petrophysics: Theory and Practice of Measuring Reservoir Rock and Fluid Transport Properties.* Gulf Professional Publishier.

Wandrey, C., Law, B., & Shah, H. (2004). Sembar Goru/Ghazij Composite Total Petroleum System, Indus and Sulaiman-Kirthar Geologic Provinces,Pakistan and India. *U.S. Geological Survey Bulletin 2208-C*.

Wang, J., Cao, J., & Yuan, S. (2020). Shear wave velocity prediction based on adaptive particle swarm optimization optimized recurrent neural network. *Journal of Petroleum Science and Engineering*, 107466.

WIDESS, M. (1973). HOW THIN IS A THIN BED? *GEOPHYSICS*, 1176-1180.

Wrona, T., Pan, I., Gawthorpe, R., & Fossen, H. (2018). Seismic facies analysis using machine learning. *Geophysics*, 83-95.

Wu, S., Nguyen, T., Liu, Y., Southam, G., Wang, S., Chan, T.-S., . . . Huang, L. (2019). Deficiencies of secondary Fe (oxy)hydroxides associated with phyllosilicates and organic carbon limit the formation of water-stable aggregates in Fe-ore tailings. *Elsevier*, 73-87.

Xu, S., & Payne, M. (2009). Modeling elastic properties in carbonate rocks. *The Leading Edge*, 66-74.

Yuedong, Q., & Hongwei , A. (2007). Study of petrophysical parameter sensitivity from well log data. *Springer*, 282-287.

Zafar , Z., Shoaib , K., Afsar , F., Raja , Z., Tanveer , A., & Burley , S. (2018). A radical seismic interpretation re-think resolves the structural complexities of the Zamzama Field, Kirther Foredeep, Pakistan. *PAPG/SPE annual technical conference*, 11–12.

Zafar, Z., Shoaib, K., Afsar, F., Raja, Z., Tanveer, A., & Burley, S. (2018). A radical seismic interpretation re-think resolves the structural complexities of the Zamzama Field, Kirther Foredeep, Pakistan. *PAPG/SPE Annual Technical Conference*.

Zafar, Z., Shoaib, K., Afsar, F., Raja, Z., Tanveer, A., & Burley, S. (2018). A radical seismic interpretation re-think resolves the structural complexities of the Zamzama Field, Kirthar Foredeep, Pakistan. *PAPG-SPE Annual Technology*.

Zaigham, , N., & Mallick, , K. (2000). Prospect of hydrocarbon associated with fossilrift structures of the southern Indus basin, Pakistan. *AAPG bulletin*, 1833- 1848.

Zhang, Y., Zhang, C., Ma, Q., Zhang, X., & Zhou, H. (2021). Automatic prediction of shear wave velocity using convolutional neural networks for different reservoirs in Ordos Basin. *Journal of Petroleum Science and Engineering*.

Zhou, H., Zhang, J., Zhou, Y., Guo, X., & Ma, Y. (2021). A feature selection algorithm of decision tree based on feature weight. *Expert Systems with Applications*, 113842.

Zhu, K.-G., Ma, M.-Y., Che, H.-W., Yang, E.-W., Ji, Y.-J., Yu, S.-B., & Lin, J. (2012). PC-based artificial neural network inversion for airborne time-domain electromagnetic data. *Applied Geophysics*, 1-8.

Zoeppritz, K. (1919). On the reflection and propagation of seismic waves. *Gottinger Nachrichten*.

DRSM- QAU